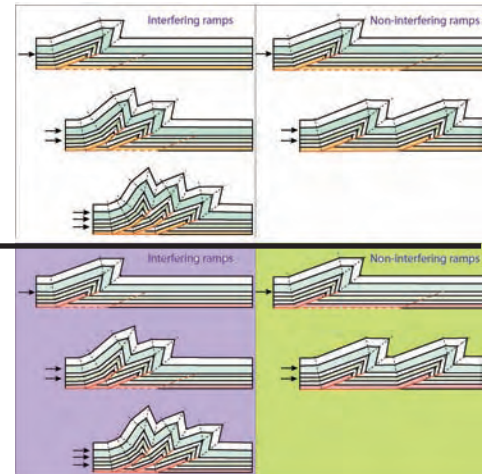# 3. Thrusts, folds and orogens

Reverse faults or thrusts are found in the following tectonic regimes:
- Contractional orogenic systems or collisional zones (metamorphic terranes in the axial parts of collisional orogens and low-grade to non-metamorphic foreland fold and thrust belts);
- Subduction zones (i.e., accretionary wedges and Andine-type orogens);
- Strike-slip systems (restraining bends, restraining step-overs);
- Inverted basins.

Folds are found in the same tectonic regimes and, in addition, in extensional settings (normal fault-propagation folds, rollover anticlines and synclines).

Thrust systems consist of one (or more) basal detachment (or decollement, or sole thrust) and more steeply dipping (often with ramp-flat geometries) thrusts or imbricate thrusts (combined into imbricate fan or duplex structures) that branch off from the basal thrust. When rocks involved in thrusting are limited to sedimentary cover, the tectonics is termed thin-skinned. When the basement rocks are involved as well, the term thick-skinned tectonics is used.

Thrust faults (figs. 21, 22, 23) normally accom-plish the following general (but reversable) rules: 1) they cut undeformed and subhorizontal sedimentary successions (unless they affect a folded succession or a pre-existing thrust or the faults occur along an unconformity, fig. 24); 2) thrusts cut upsection; 3) they propagate in the direction of transport (unless out of sequence thrusts develop, fig. 25).

Thrust faults are regularly associated in thrust fault systems that can be of two types: 1) Duplexes (fig. 26), bounded to the top and to the bottom by roof and floor thrusts respectively; depending on the relationship between fault spacing and displacement, hinterland dipping duplexes (when displacement is smaller than ramp spacing), antiformal staks (when displacement equals ramp spacing) and foreland dipping duplexes (when displacement is larger than ramp spacing) may develop. 2) Imbricate fans (figs. 27, 28, 29, 30, 31, 32), characterised by the absence of a roof thrust.

Thrust faults and thrust fronts of orogenic belts are often laterally segmented. Faults that locally link segmented thrusts are called transfer faults (figs. 34, 35). Displacement may be, however, transferred also by diffuse strain. In this case the term transfer zone is adopted.

The spacing between successive thrust faults in fold-and-thrust belts is controlled by the thickness of the sediments entering the belt at the deformation front (figs. 36, 37).

The geometry of the wedge is controlled by friction along the basal decollement. Highly frictional decollements are associated to narrow belts with a steep topographic slope. Low friction decollement are associated to wide and flat mountain belts (fig. 38). These characters are well documented in the Zagros that display different geometries of the wedge in areas characterised by absence or occurrence of Cambrian salt (figs. 39, 40).

In foreland belts, thrust faults produce folding (figs. 41-45). Folds created by thrust faulting are called forced folds and can be of three types (figs. 46-75): 1) fault-bend faults, generated when the hangingwall of a thrust sheet pas-

ses over a stepped (ramp-and-flat) thrust fault. Above each kink of the thrust fault surface folds are generated to accommodate slip; 2) fault-propagation folds, generated by folding strain at the tip of the ramp of a blind thrust, where displacement dies to zero; 3) detachment folds, generated above the tip line of a thrust that developed along a bedding-parallel detachment surface (i.e., along a flat).

Another structure typical of fault-and-thrust belts are triangle structures (figs. 76-88), also called structural wedges. They develop according to the conjugate faulting theory and consist of two connected fault segments that bound a triangular block. The two faults may be either two ramps or a ramp and a detachment. Slip occurs along both faults allowing propagation of the wedge and determining the folding of the hangingwall.
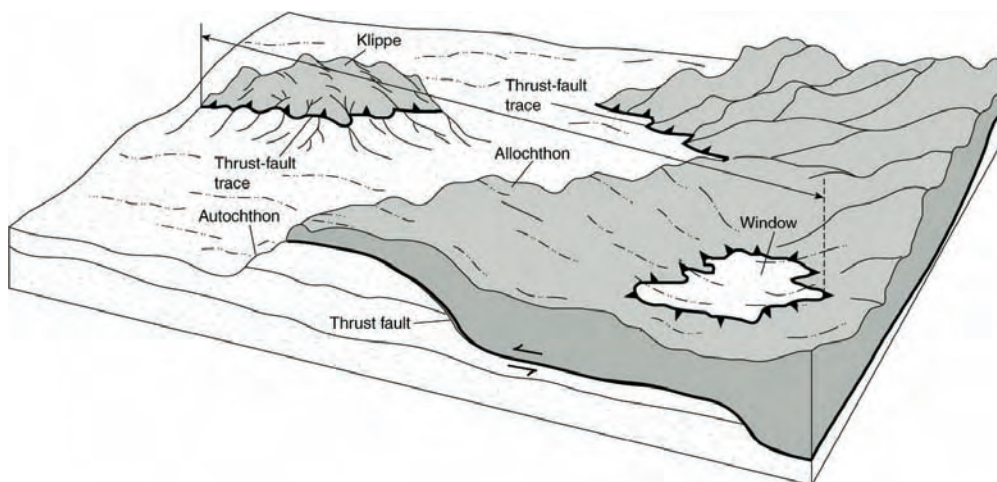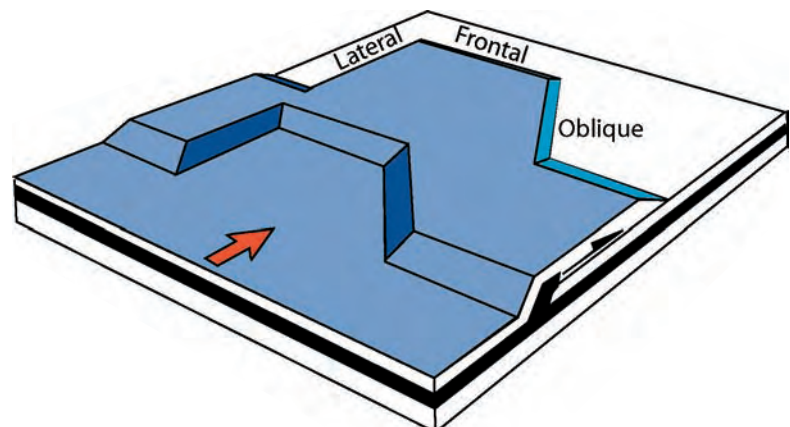

Fig. 21 - Basic nomenclature of thrust fault systems. Upper panel after TWISS & MOORES, 1992.
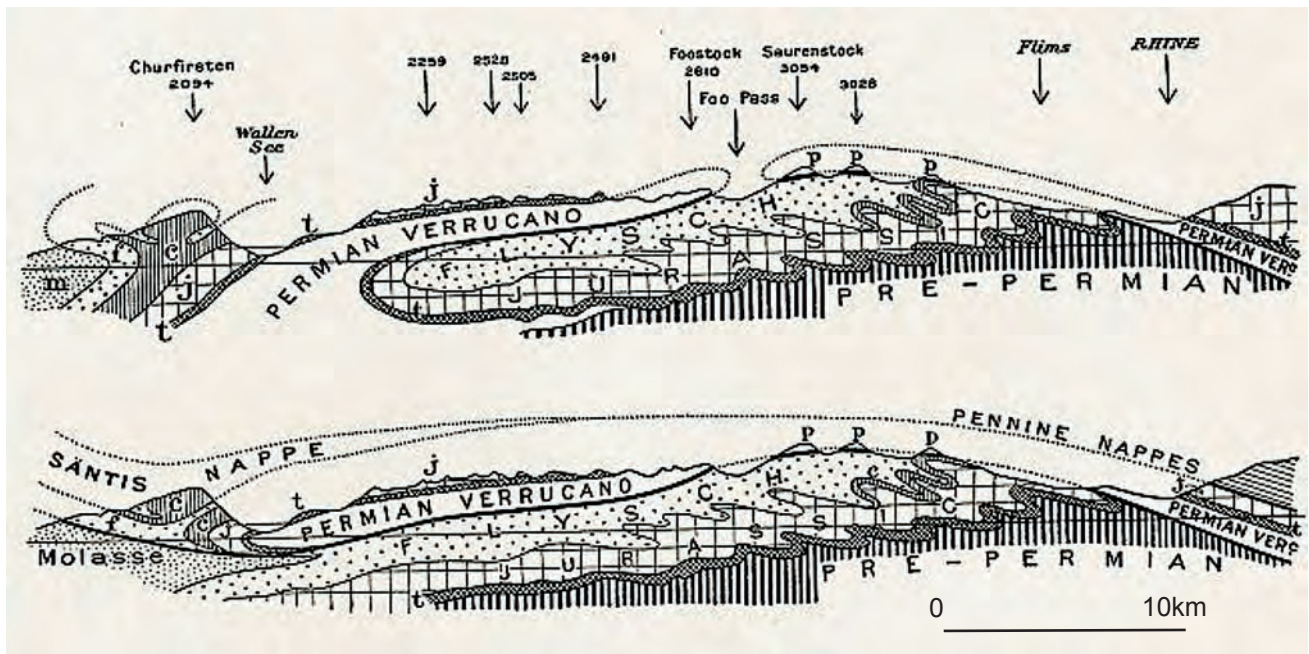
Fig. 22 - Upper panel. Glarus thrust, Swiss Alps. The dark rocks above the thrust (the Permian Verrucano Fm.) have been emplaced on the lighter Mesozoic limestones. Lower panel. Although the age and nature of the lithologies was recognised since the early beginning, the tectonic nature of the contact (by thrust fault) was only later recognised. To explain the regional geology of the Glarus area, Arnold Escher (1807-1872) and his student Albert Heim (1849-1937) proposed a strange "double fold" structure. Heim's clear descriptions in his classic 1878 text on mountain building led, in 1884, to the re-interpretation of the Glarus structure as a single, southward-derived thrust sheet by Marcel Bertrand (1847-1907) - although Bertrand had never visited the area. (after Butler, 2006; earth.leeds.ac.uk/tectonics/thrust_tectonics/index.htm).

Fig. 23 - Possible 2-D geometries of thrust faults. The thrust can either reach the Earth's surface or not (blind faults). Note the staircase (ramp and flat) geometry of the fault plane. Redrawn after McCLAY (1992).
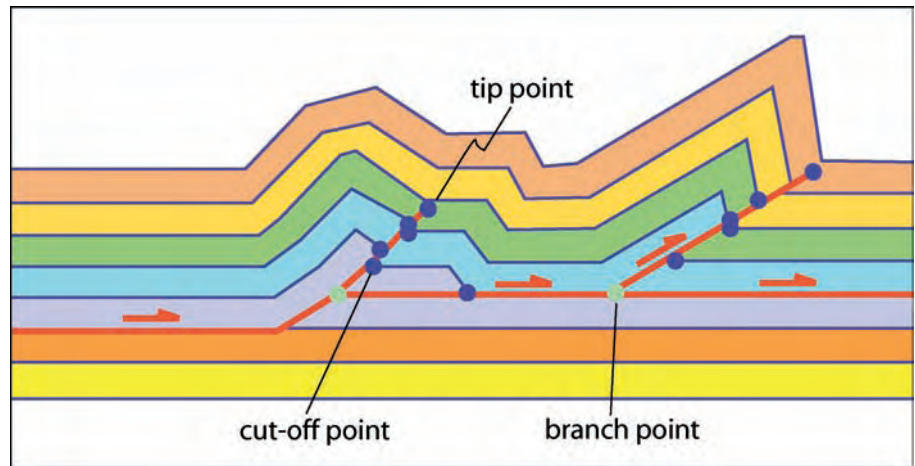

Fig. 24 - Generally older thrusts are carried on younger thrusts (in sequence thrusting). Higher older thrusts become folded as younger thrusts climb ramps. The opposite occurs when out-of-sequence thrusts develop. Redrawn after McCLAY (1992).
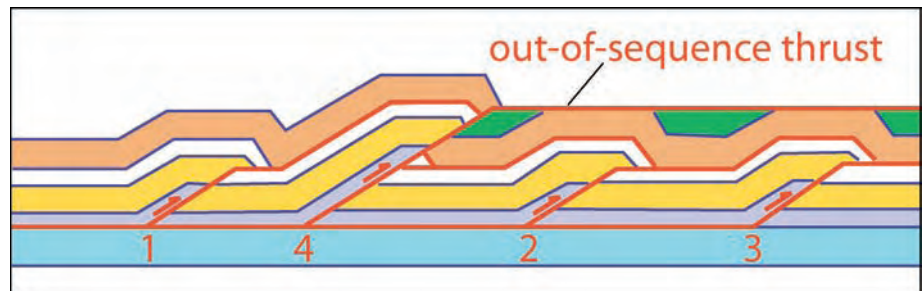

Fig. 25 - In a fold-and-thrust belt the sense of transport along thrust faults is generally towards the foreland (fore-thrusts). In some thrust faults (named backthrusts), however, the sense of transport may be toward the hinterland. The combination of thrusts and backthrusts determine the development of pop-up structures (after http://earth.leeds.ac.uk/assynt-geology/geology/thrusts/what/backt hrust.htm).
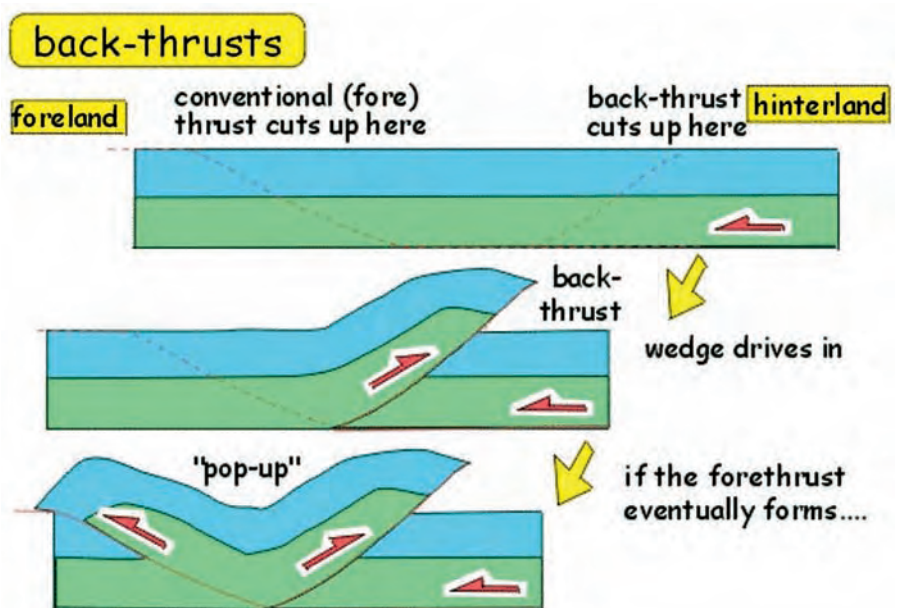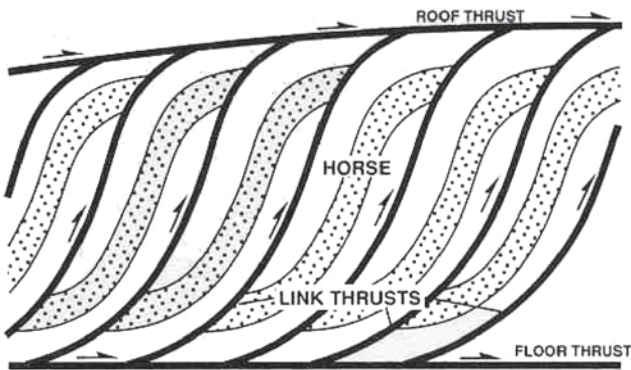
Fig. 26 - Duplexes are one of the two major geometries of thrust-fault systems. They are bounded to the top and to the bottom by roof and floor thrusts respectively. Depending on the relationship between fault spacing and displacement, three different duplex geometries may develop: hinterland dipping duplexes (when displacement is smaller than ramp spacing), antiformal staks (when displacement equals ramp spacing) and foreland dipping duplexes (when displacement is larger than ramp spacing). After RAMSAY & HUBER (1987).

A. Hinterland dipping duplex
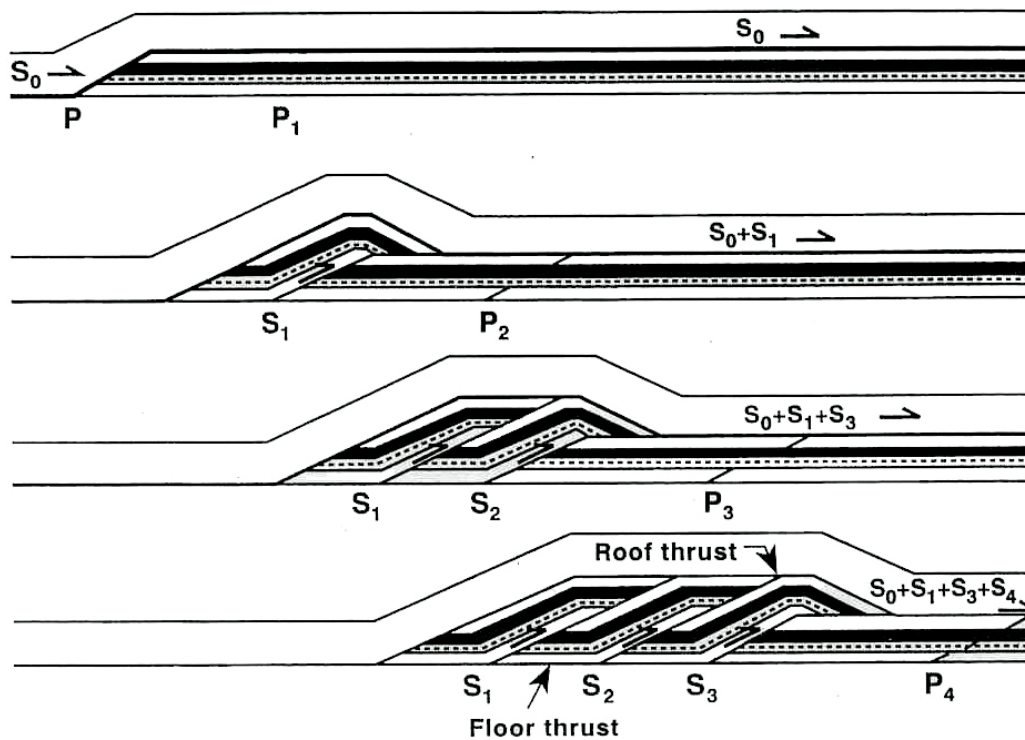
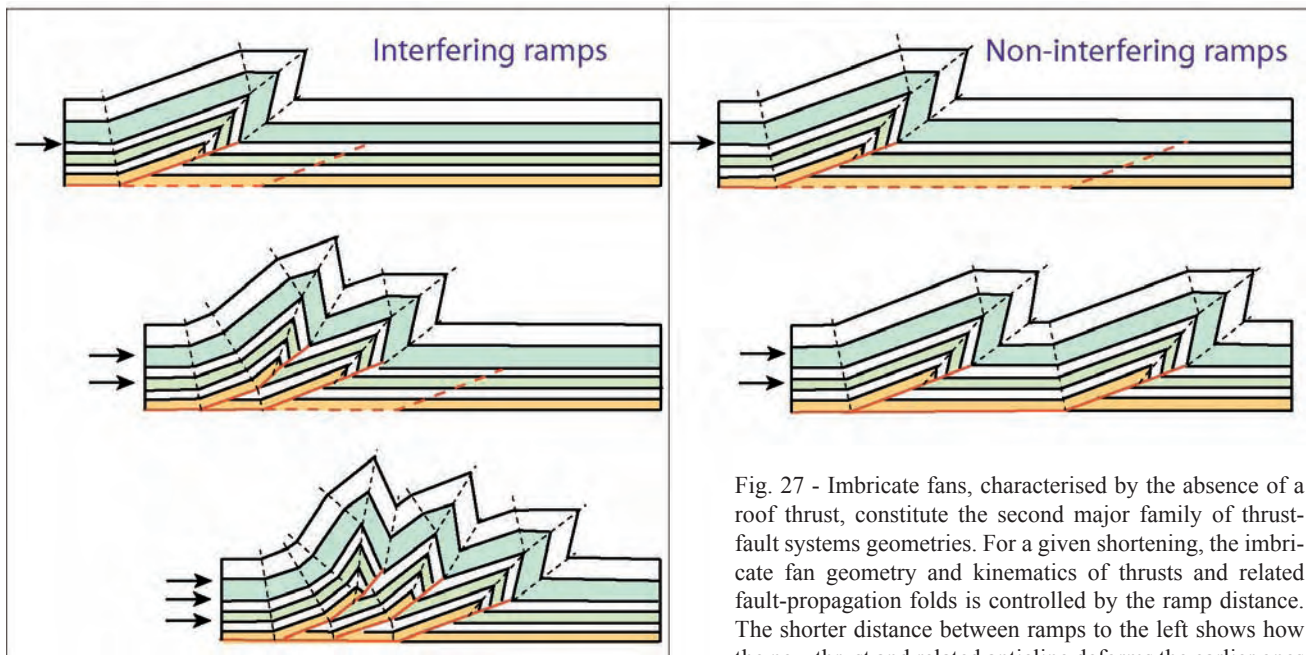## B. Antiformal stack
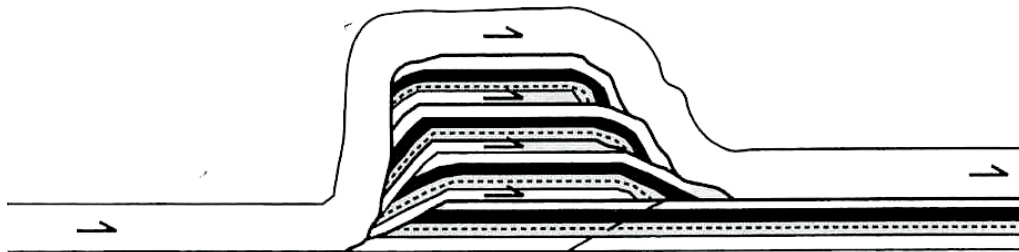
C. Foreland dipping duplex
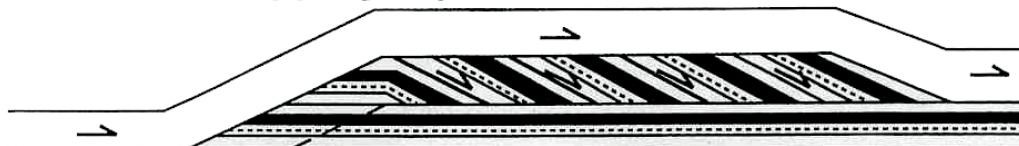
Fig. 27 - Imbricate fans, characterised by the absence of a roof thrust, constitute the second major family of thrust-fault systems geometries. For a given shortening, the imbricate fan geometry and kinematics of thrusts and related fault-propagation folds is controlled by the ramp distance. The shorter distance between ramps to the left shows how the new thrust and related anticline deforms the earlier ones (cases 2 and 3) transporting in a piggy-back sequence, plus rotating and steepening the earlier axial planes and thrust surfaces. In the example to the right, the wider distance between ramps occurs in lower friction decoupling surfaces, and maintains the original shape of the fold (after MITRA, 1986).
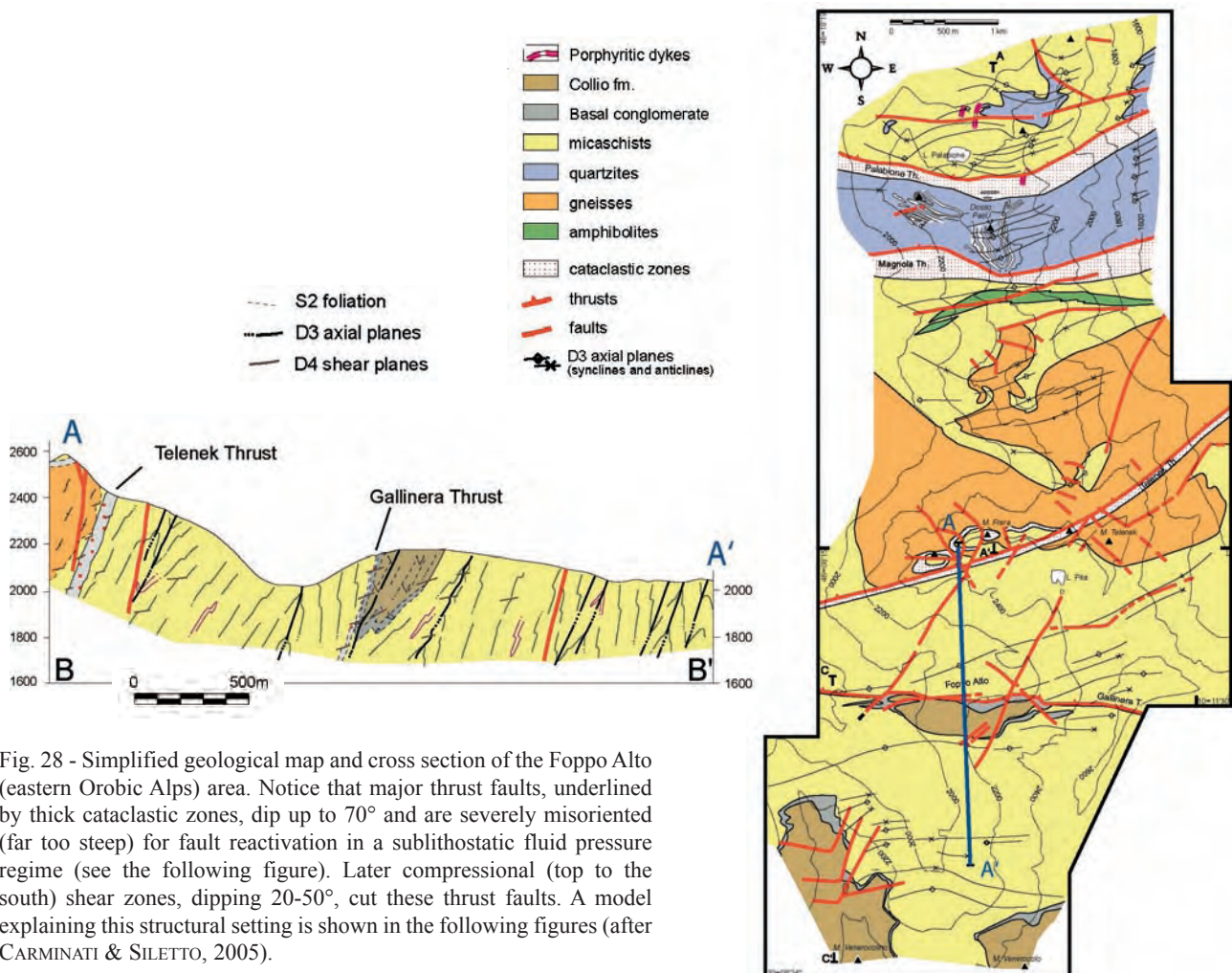

Fig. 28 - Simplified geological map and cross section of the Foppo Alto (eastern Orobic Alps) area. Notice that major thrust faults, underlined by thick cataclastic zones, dip up to 70° and are severely misoriented (far too steep) for fault reactivation in a sublithostatic fluid pressure regime (see the following figure). Later compressional (top to the south) shear zones, dipping 20-50°, cut these thrust faults. A model explaining this structural setting is shown in the following figures (after CARMINATI & SILETTO, 2005).
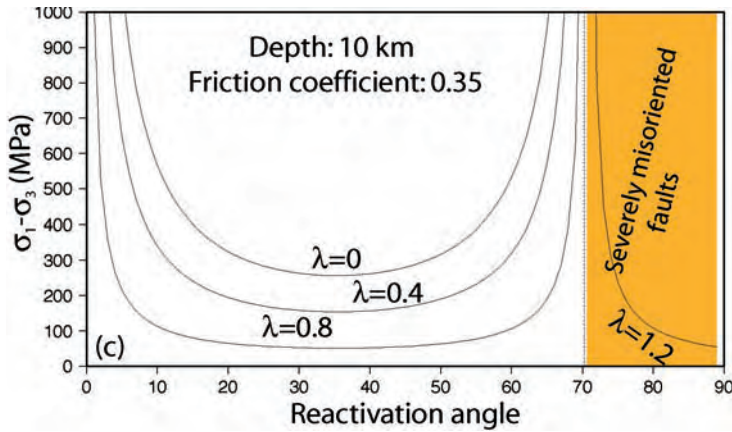
Fig. 29 - Plot of differential stresses needed in order to reactivate thrust faults with different dips at a depth 10 km for variable pore fluid pressure ratios (λ=Pf/Pl, where Pf is the fluid pressure and Pl is the lithostatic pressure). The coefficient of friction is 0.35. Notice that, even for very high fluid pressure, thrust faulting along planes more inclined than ca. 70° would need far too high differential stresses. Such faults are therefore severely misoriented to be re-sheared in a compressional regime (after CARMINATI & SILETTO, 2005).
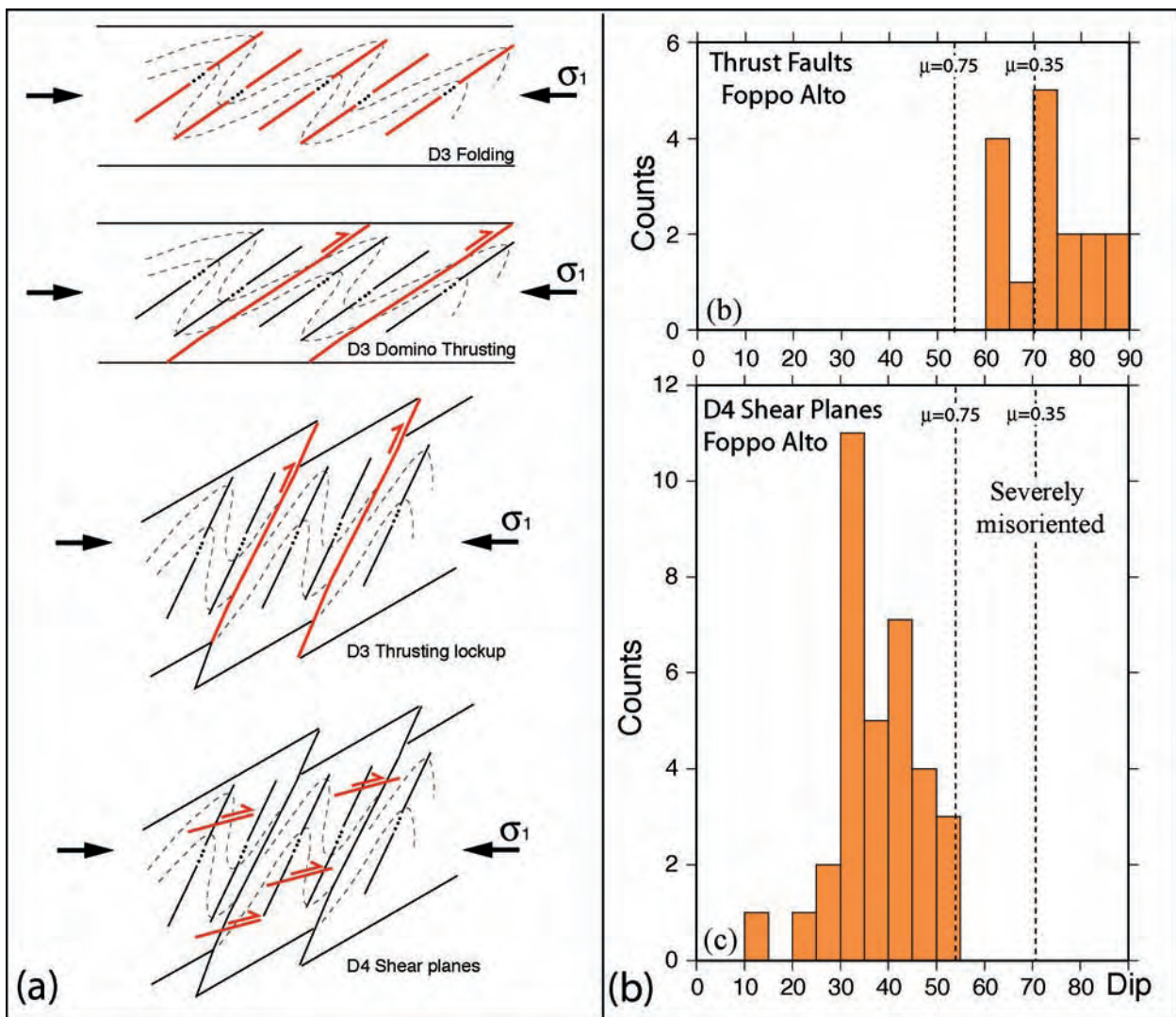

Fig. 30 - a) The thrust faults of the Foppo Alto area are severely misoriented (far too steep; see previous figures) for fault reactivation in a sublithostatic fluid pressure regime. Thrust motion likely started when the faults were less steep and the faults were progressively rotated up to the present day dip by domino tilting. When the faults became inclined beyond the fault lock-up angle, no further thrusting was accommodated along them. At later stages regional shortening was accommodated by newly formed lower angle shear planes (dipping around 30°-40°), consistently with predictions from fault mechanics. b) Dip distribution for the thrust faults and for the later (D4) shear planes of the Foppo Alto area (after CARMINATI & SILETTO, 2005).

Fig. 31 - Erosion may remove any indication of a roof thrust in a duplex thrust system, making it difficult to distinguish it from an imbricate fan. Redrawn after McClay (1992).
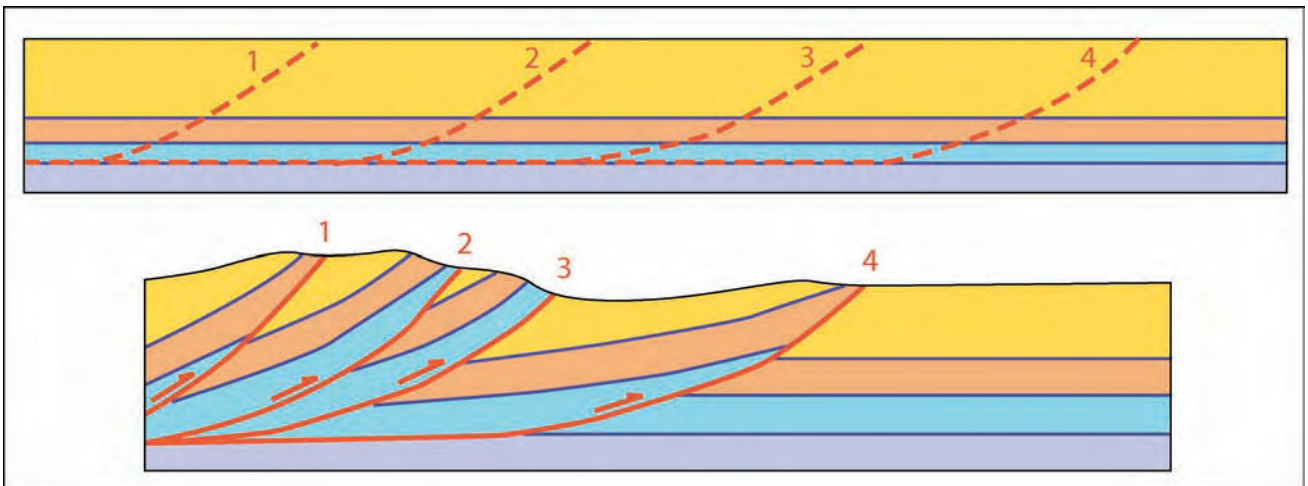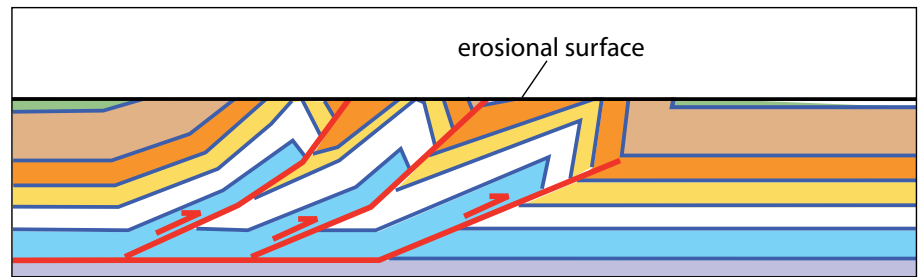

Fig. 32 - The different spacing of thrust fault ramps in the lower panel may be misinterpreted as the result of a variable spacing of fault nucleation points. When the section is retro-deformed, in this case the original spacing was constant, which is not the rule. The variable spacing in the deformed section is related to the variable displacement along the faults.
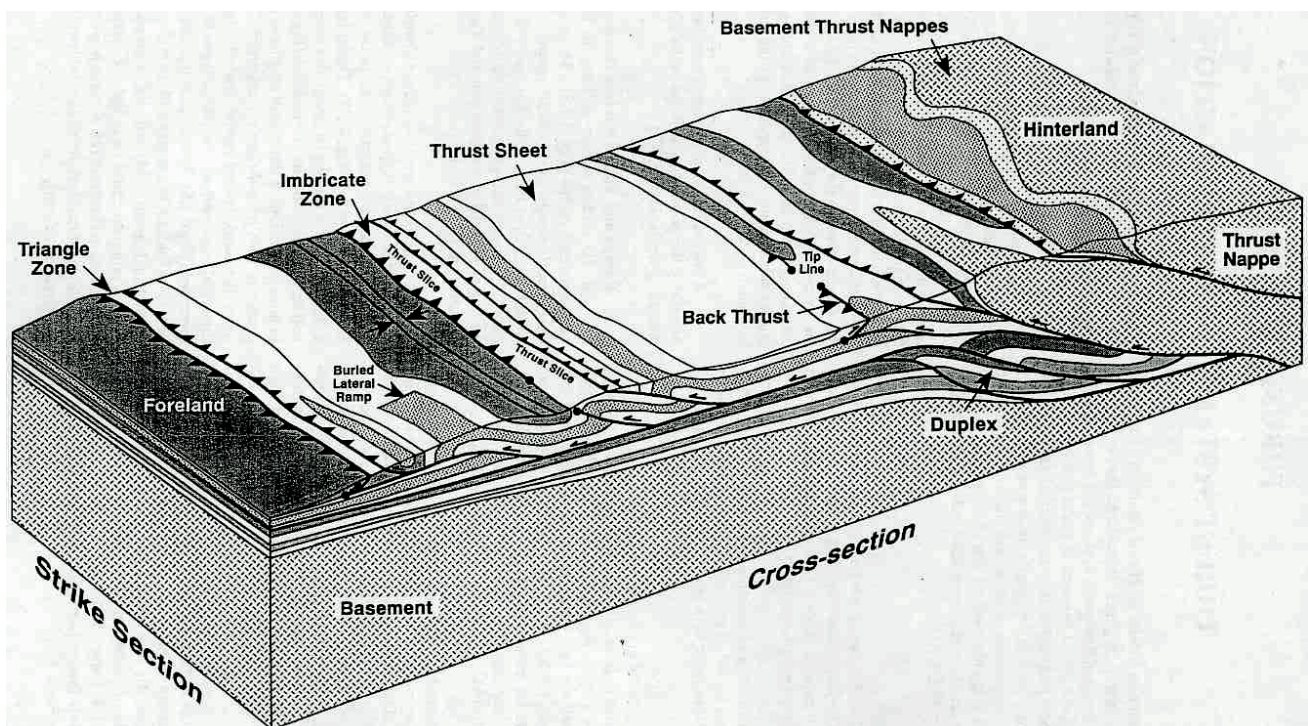

Fig. 33 - Thrust systems may be extremely complicated and all the structures so far described may coexist in fold-and-thrust belts (after De Paor, 1988).
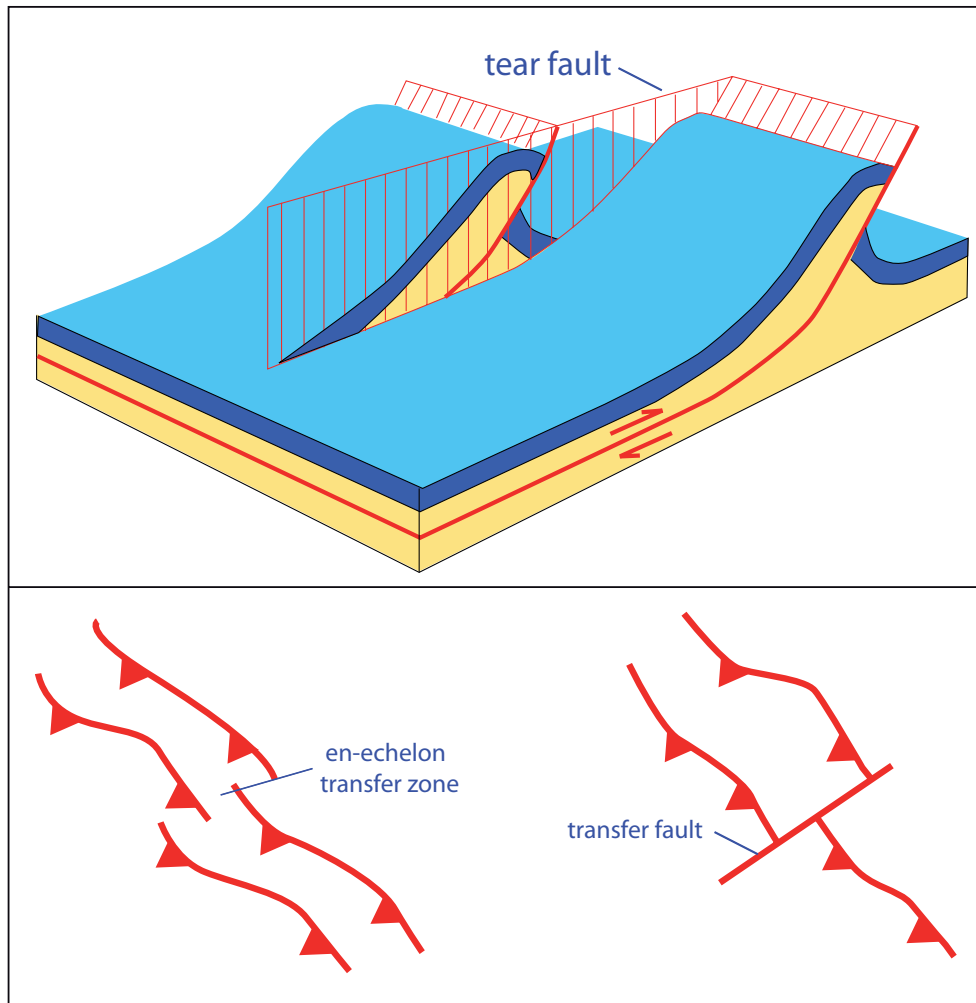
Fig. 34 - Thrust faults are normally laterally segmented. Local faults segmenting thrusts are called tear faults. At regional scale, the thrust faults may be segmented by a single fault (transfer fault) or displacement may be transferred laterally to other faults along tranfer zones (modified after TWISS & MOORES, 1992).
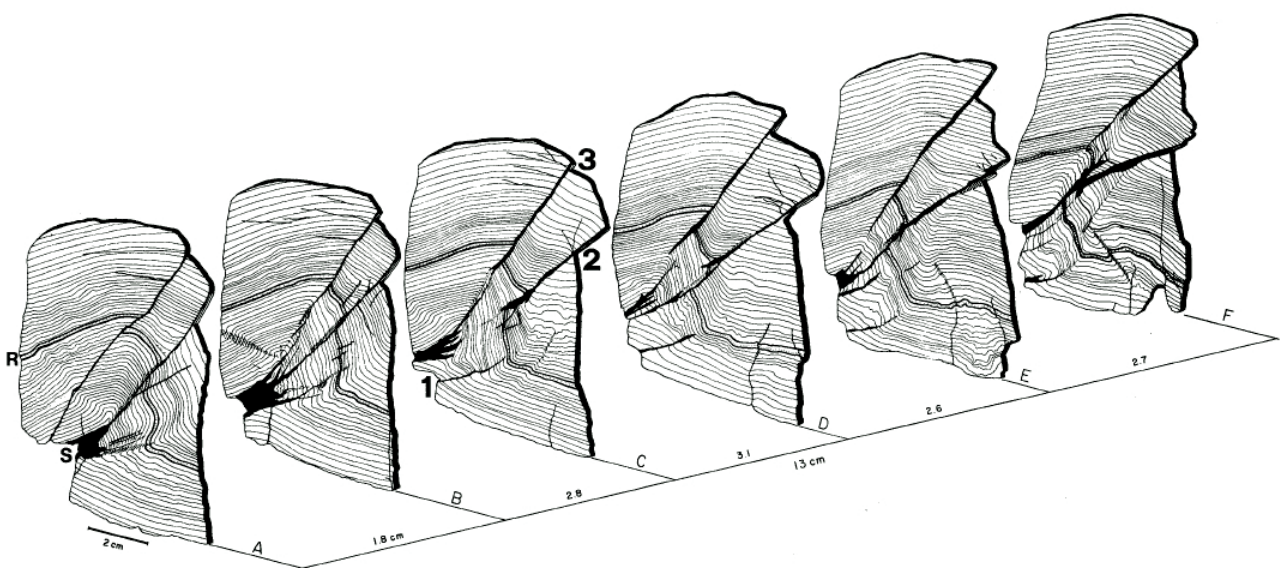

Fig. 35 - Small-scale example of transfer zones. A 30 cm wide kink-band has been cross-cut, showing how each single slice has different geometries, number of thrusts, distance among them, etc. Similar along strike variations typically occur along fold and thrust belts.
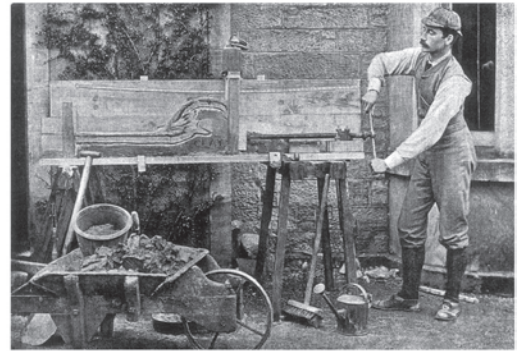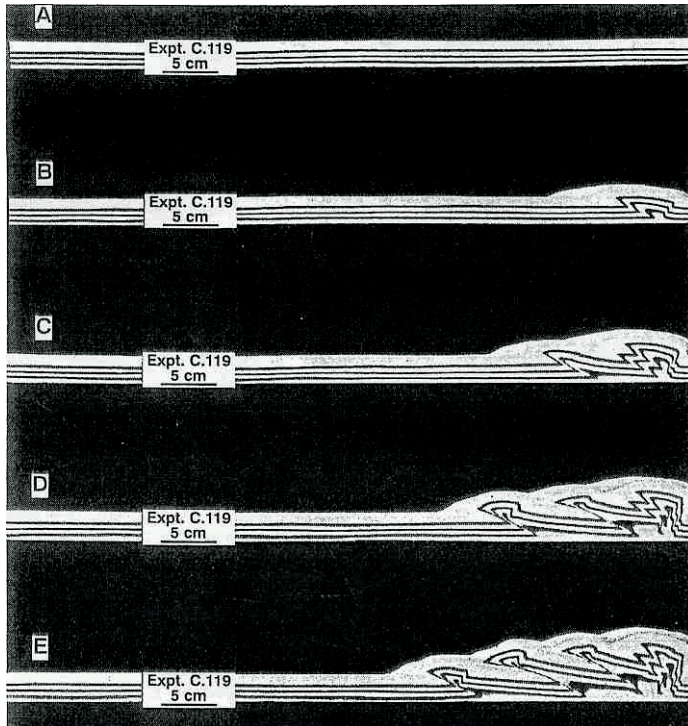
Fig. 36 - The progressive development of fold-and-thrust belts has been studied extensively (since the pioneering work of CADELL 1889, above picture) with analogue models that simulate thrust faults formation pushing laterally a multilayer of sand (plus additional materials). Notice in the left panel the foreland propagation of thrust faulting. When new thrust faults form, older thrusts are abandoned, rotated and transported passively toward the foreland (after HUIQI *et alii*, 1992).
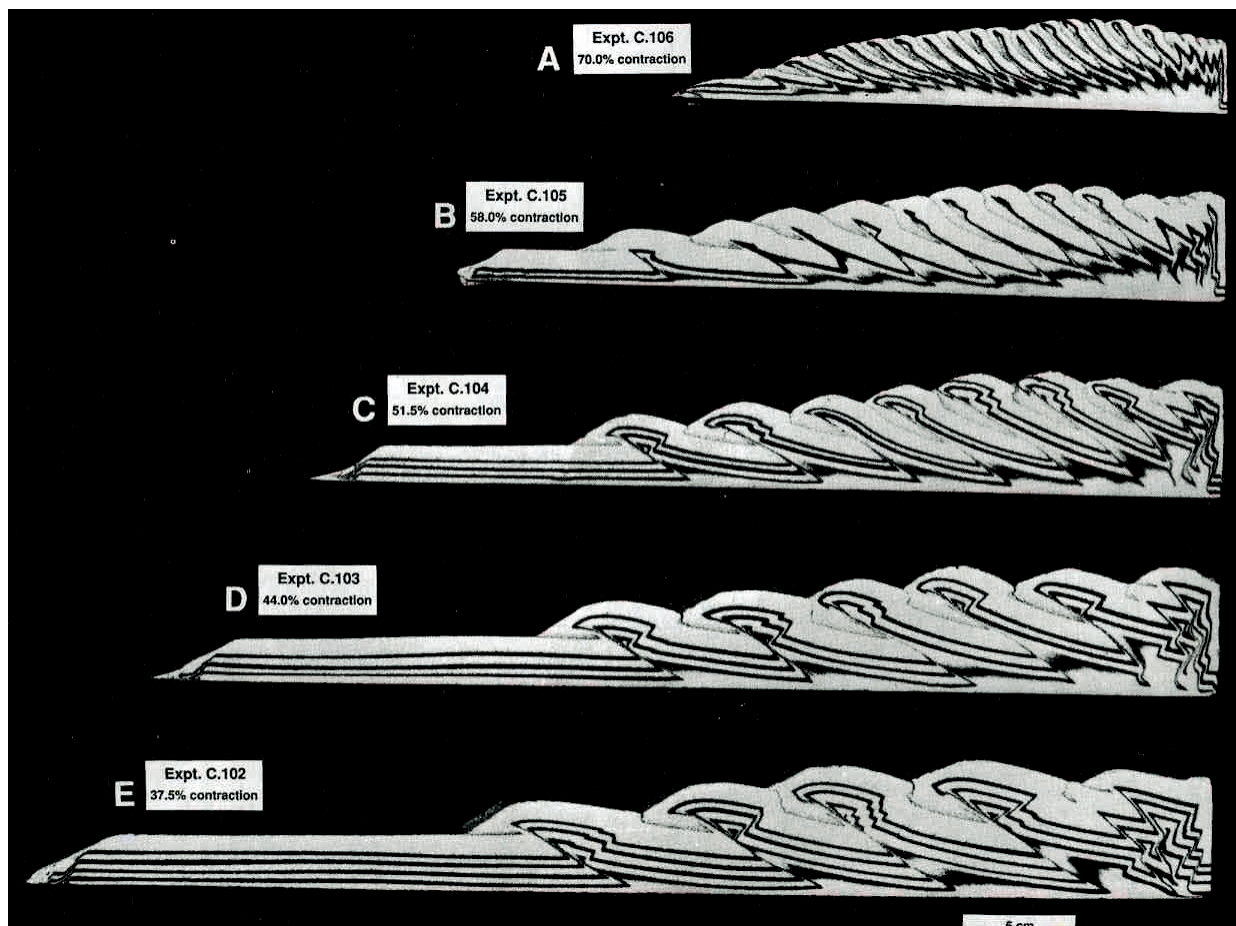

Fig. 37 - The spacing of thrust faults is controlled by the thickness of the foreland sedimentary cover above the basal decollement. The larger the thickness, the larger the spacing (after HUIQI, *et alii* 1992).
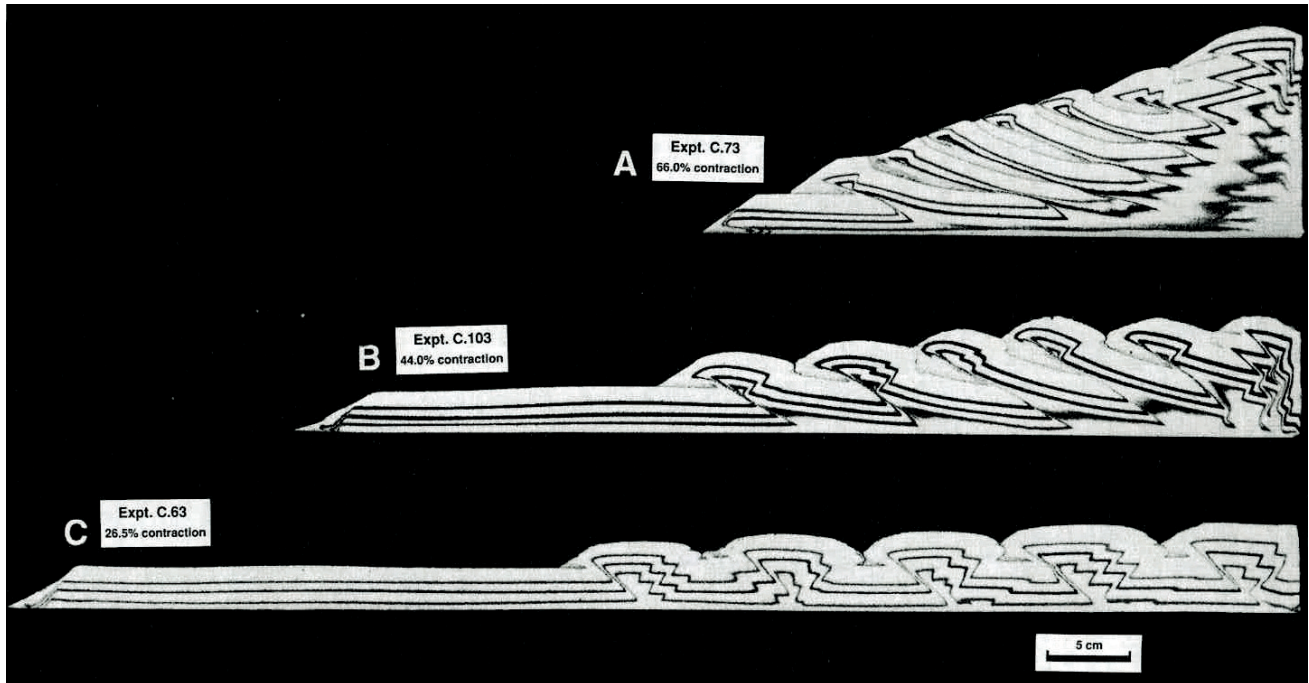
Fig. 38 - The geometry of the wedge is controlled by the friction along the basal decollement. Highly frictional decollements are associated to narrow belts with a very steep topographic slope. Low friction decollements are associated to wide and flat mountain belts. In experiments a-c, the friction coefficient of the decollement is 0.55, 0.47 and 0.37 respectively. Compare these geometries with the following two figures.
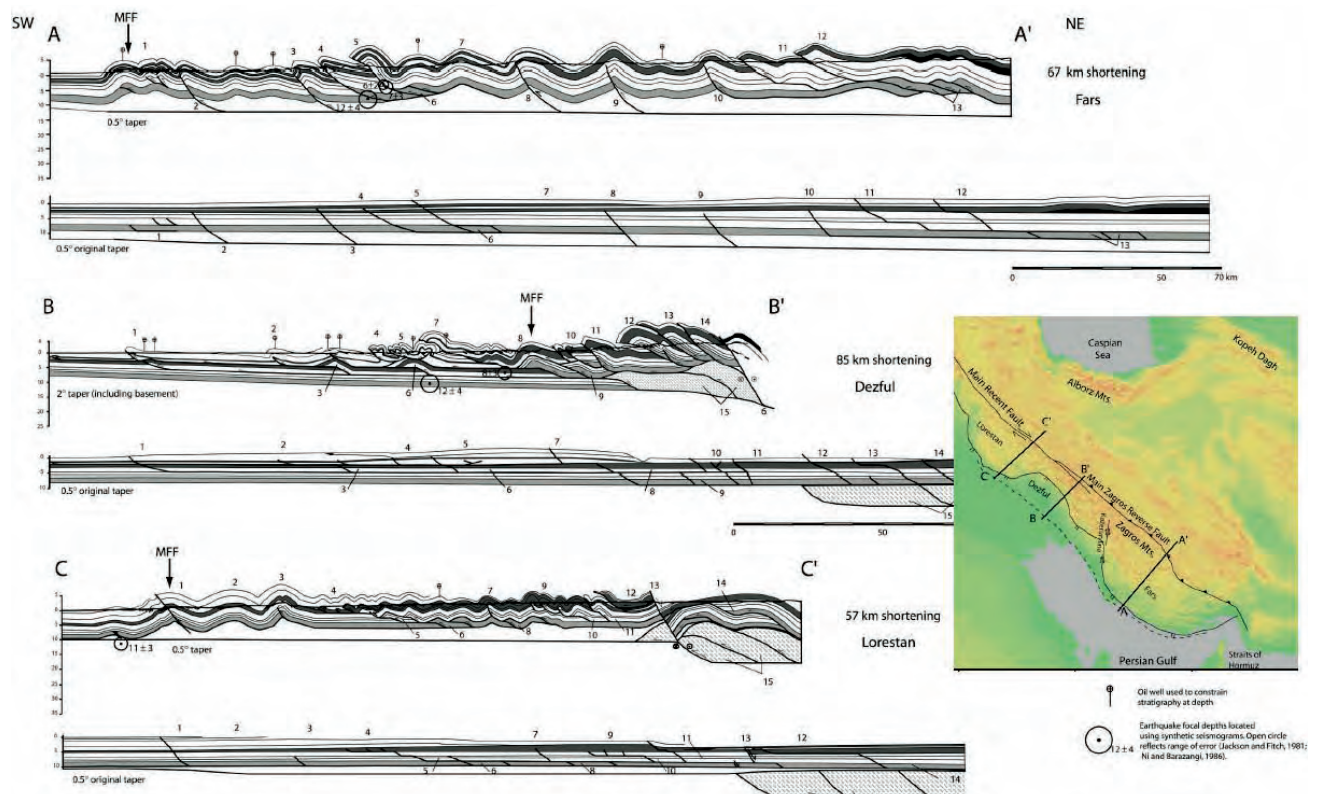

Fig. 39 - Three cross sections through the Zagros show different fold-and-thrust geometries. The basal decollement of sections A and C runs through the Cambrian Hormoz Fm. (salt) and the chain is wide. Along section B no salt occurs along the basal decollement and the surface slope is steeper and the belt is narrower with thrust faults characterised by larger displacement (after McQuarrie, 2004).
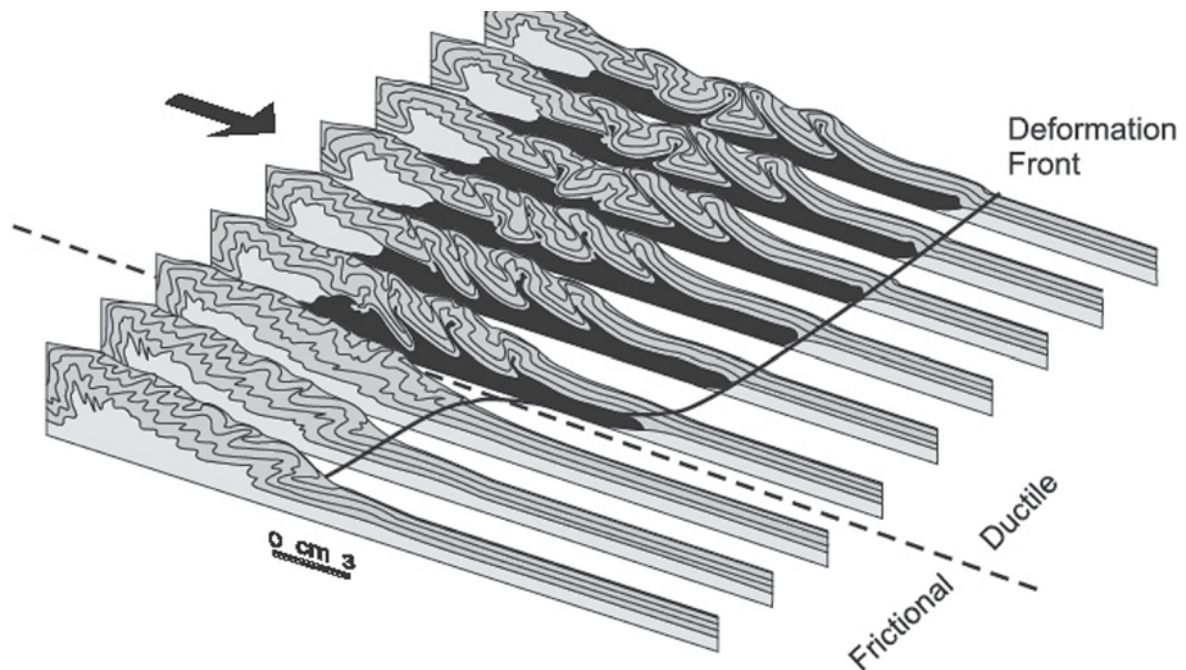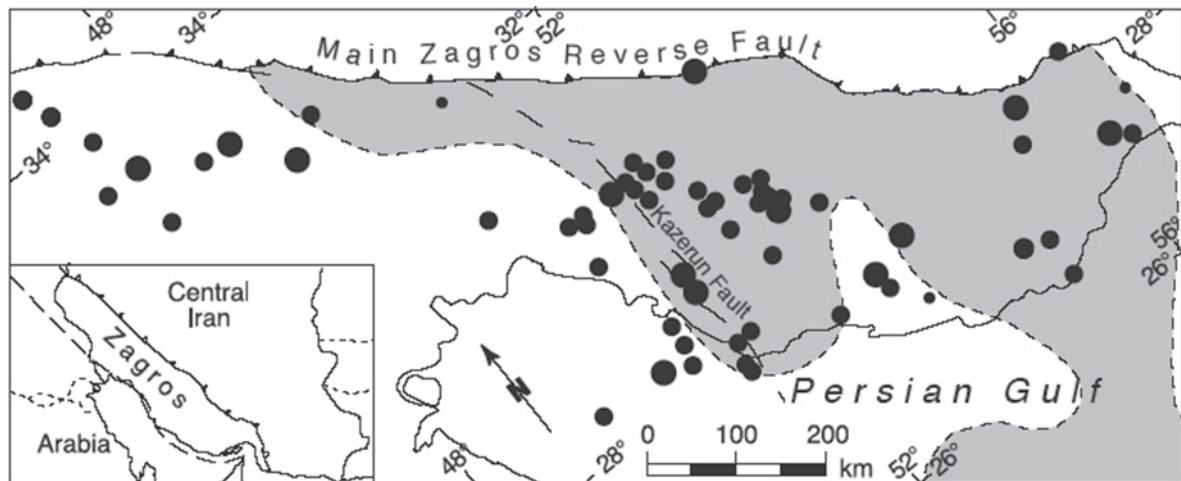
Fig. 40 - Upper figure: In the portion of the Zagros shortened above a low-friction ductile decollement (rock salt, grey area), low- to moderate-magnitude earthquakes (Mw = 5.3-5.6), distributed over a wide area, occur along several long-lived thrust faults. Conversely, in areas shortened above high-friction decollements large-magnitude earthquakes (Mw = 6.6 - 6.8), distributed over a narrow zone are likely to occur along few short- lived thrust ramps (after KOYI *et alii*, 2000).

Lower figure: Above the ductile domain, both forward- and rearward-vergent thrusts form, whereas above the frictional domain, only forward-vergent thrusts prevail. The thrust belt is characterised by salients above ductile decollements and by recesses above frictional layers (after COTTON & KOYI, 2000).
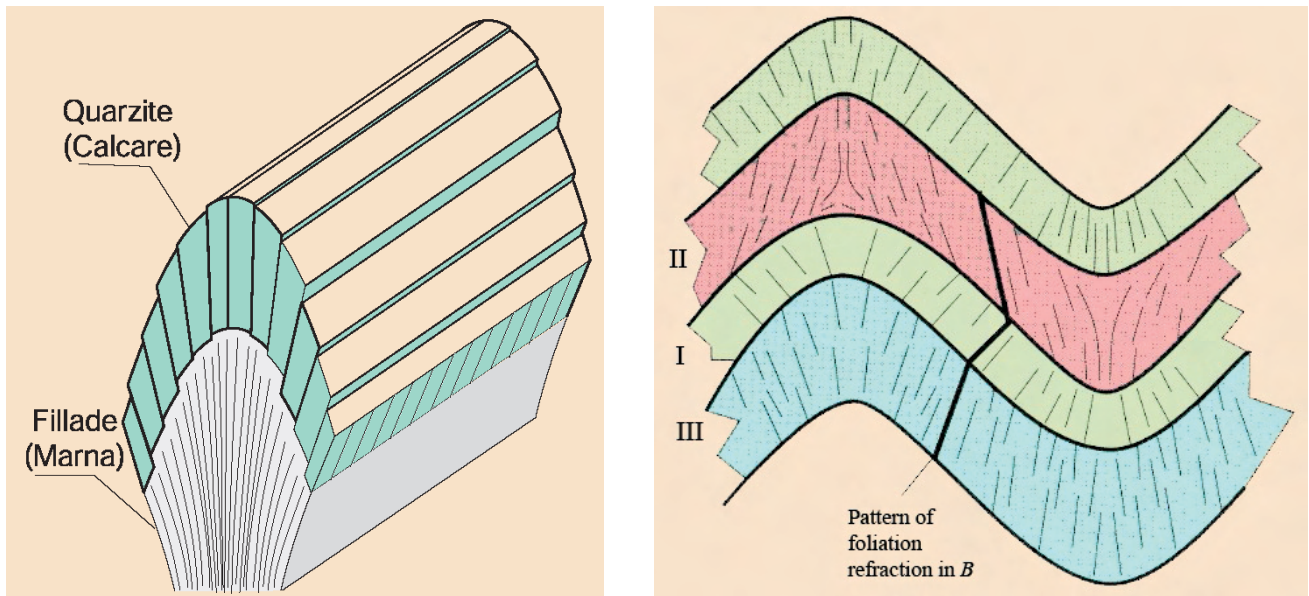
Fig. 41 - Cleavage formation is often associated to folding. When cleavage is subparallel to fold axial planes it is termed axial plane cleavage. However, the axial plane cleavage is often refracted between competent and incompetent layers and the spacing is dependent on lithology (larger in more competent lithologies). Cleavage may represent an important source for rock permeability. Modified after TWISS & MOORES (1992).

Fig. 42 - Folded volcaniclastic rocks of the Permian Collio Fm. (the original stratigraphic layers are indicated by the black line). Notice the development of a strong axial plane cleavage (red lines) that is unevenly distributed. Some layers (normally those characterised by higher percentages of phyllosilicates, such as micas for example) are characterised by a sharp cleavage, whereas in other layers (more competent) cleavage is absent. In some layers, cleavage may have obliterated continuously the original strata. Val Belviso, Central Southern Alps.
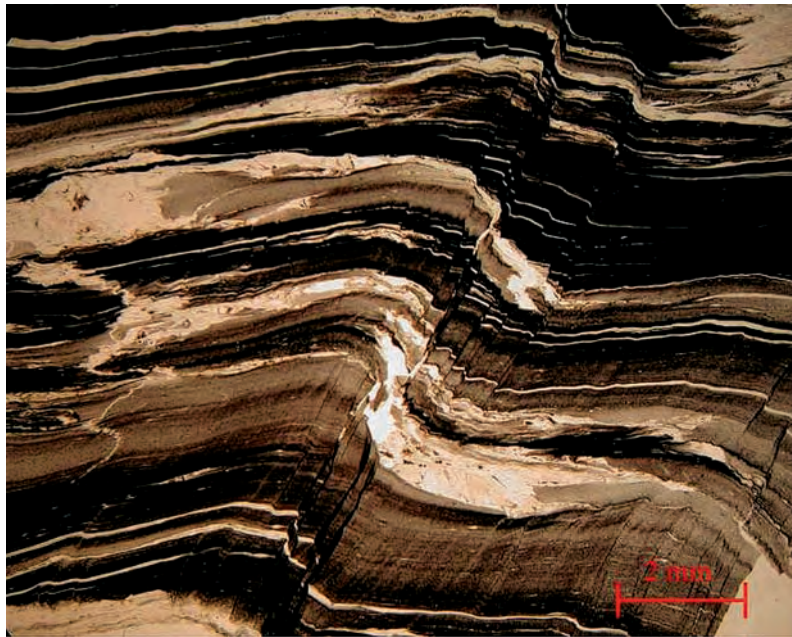
Fig. 43 - Microphotograph of an axial plane cleavage developed in marly limestones from the Alpi Apuane, Central Italy. Notice that one of the main processes controlling cleavage development in this sample was pressure solution.
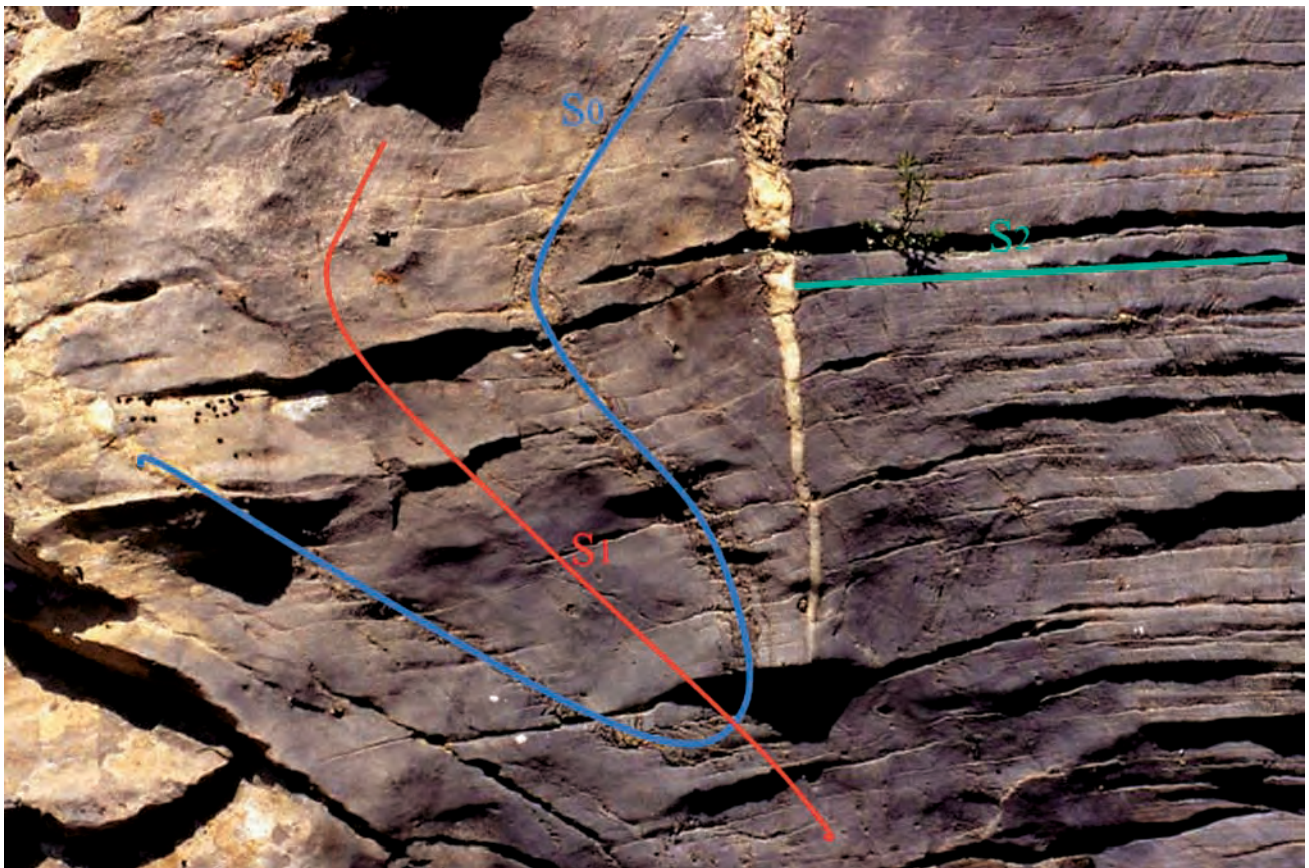

Fig. 44 - In terrains involved in more than one phase of folding, different generations of cleavage may develop. For example in these Cretaceous marly limestones from the Mt. Marguareis area (Ligurian Brianconnais, Western Alps) two generations of folds and corresponding axial plane cleavages (labelled as S1 and S2) can be observed. The original stratigraphic surfaces are labelled S0.
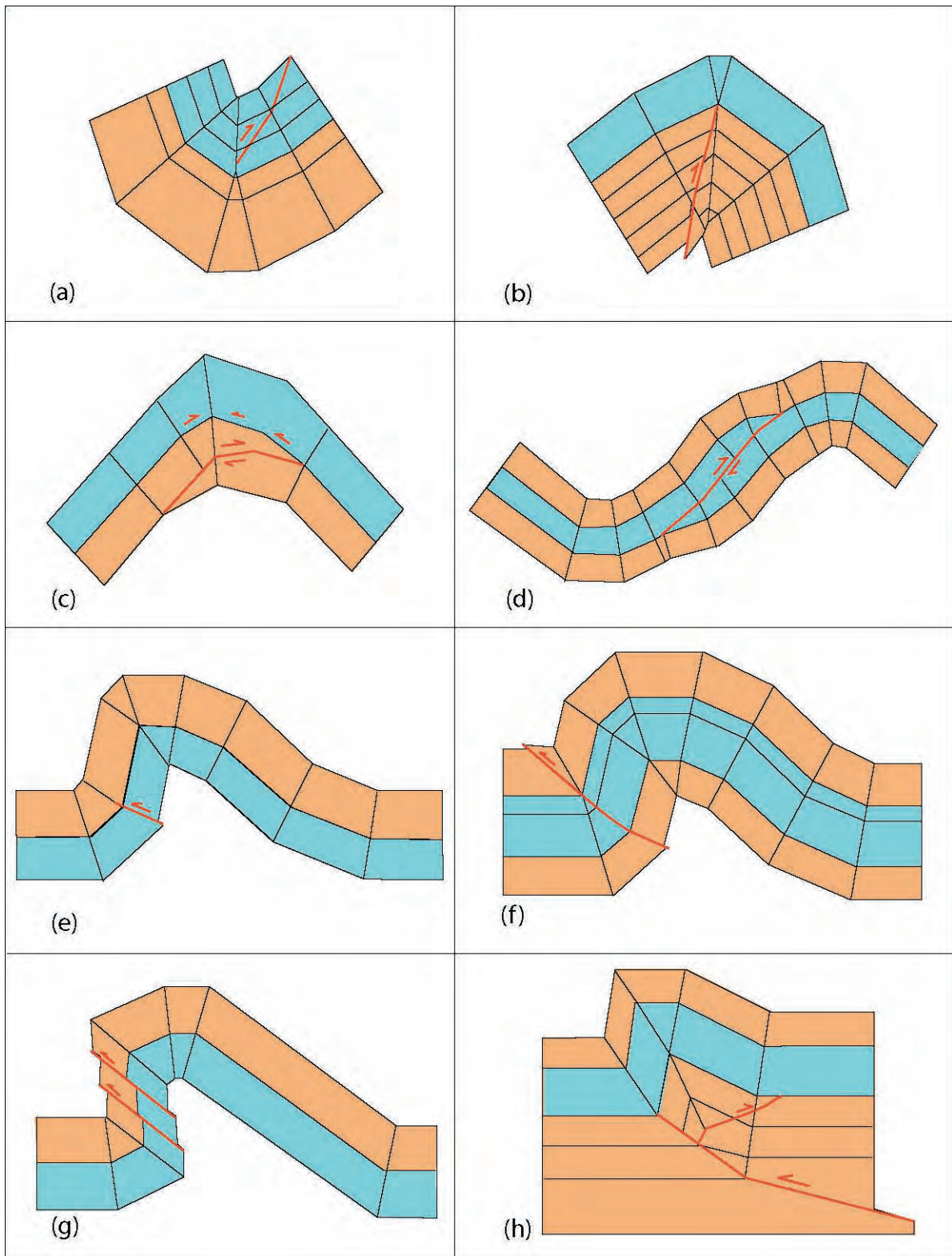
Fig. 45 - Normally folding is induced by thrusting. At shallow levels, however, rocks display brittle behaviour during folding and minor faults associated to folding may form. Common types of fold-accommodation faults: (a) out-of-syncline thrust propagating on the gently dipping limb; (b) into-anticline thrust propagating on the gently dipping limb; (c) hinge wedge thrust; (d) limb wedge thrust; (e) forelimb space accommodation thrust; (f) forelimb-backlimb thrust; (g) forelimb shear thrusts; (h) back thrust (after MITRA, 2002).
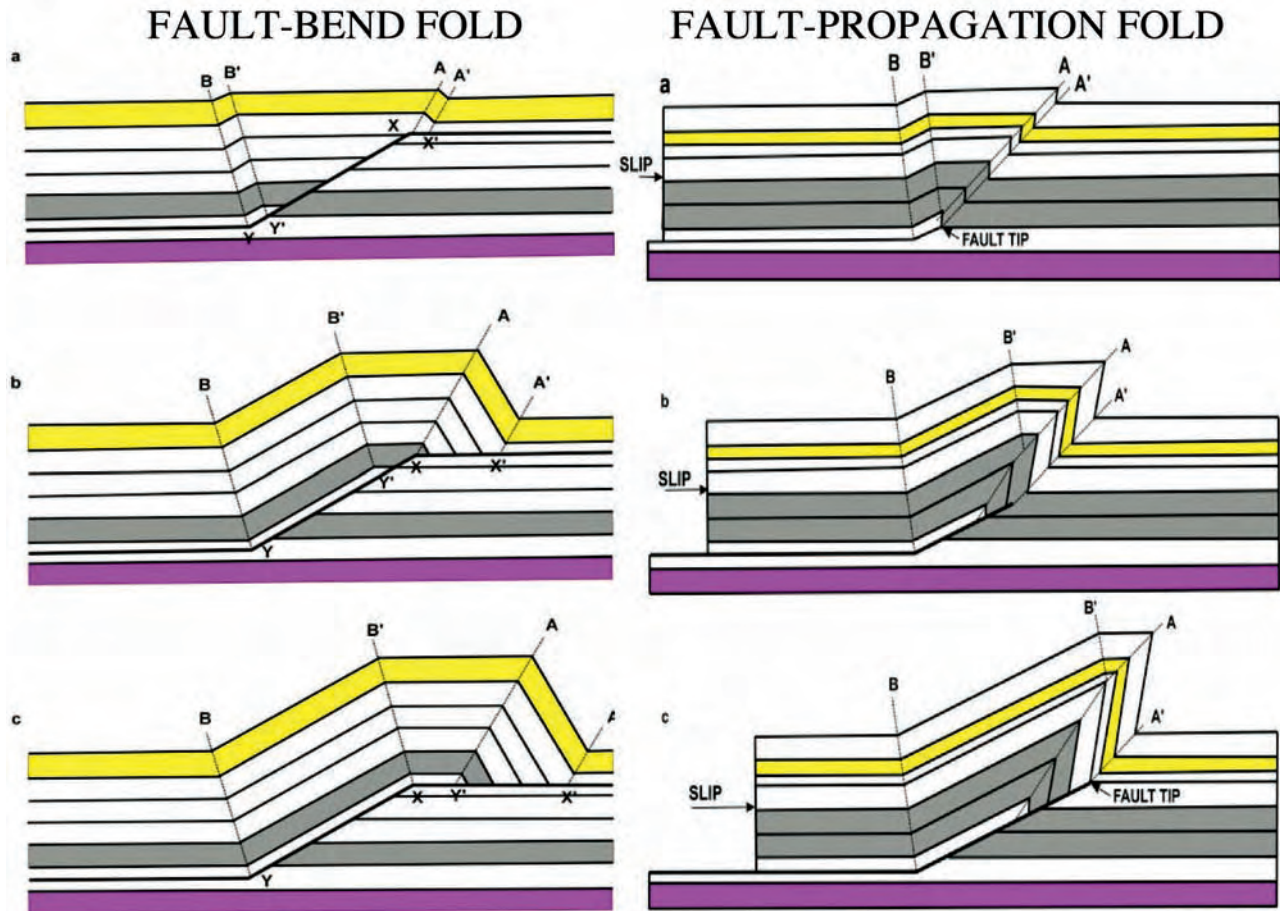
FAULT-BEND FOLD

FAULT-PROPAGATION FOLD

Fig. 46 - Classic relations between thrust shape, propagation and fold development (SUPPE, 1983; 1985). In both cases the back-limb of the fold is parallel to the footwall ramp. Fault-bend folds are generated when the hangingwall of a thrust sheet passes over a stepped (ramp-and-flat) thrust fault. Above each kink of the thrust fault surface folds are generated to accommodate slip.

Fault-propagation folds are generated by the folding strain at the tip of the ramp of a blind thrust, where displacement dies to zero. Above this point, an asymmetric fold with a steep or overturned forelimb (indicating the vergence of the thrust) is formed. With the progressive upward migration of the thrust fault tip, the fold may be dissected and in part transported in the hangingwall of the thrust sheet, with a relict footwall syncline. The forelimb is less inclined in the fault-bend fold, whereas it is often overturned and subject to elongation and flattening in fault-propagation folds.
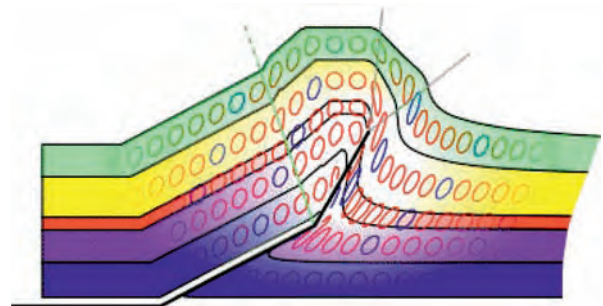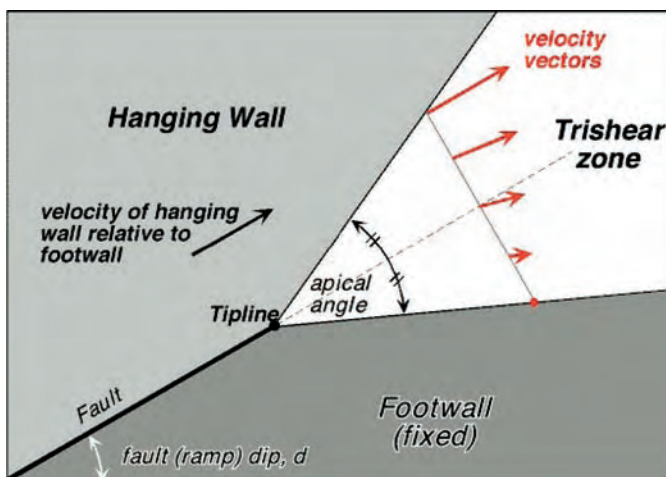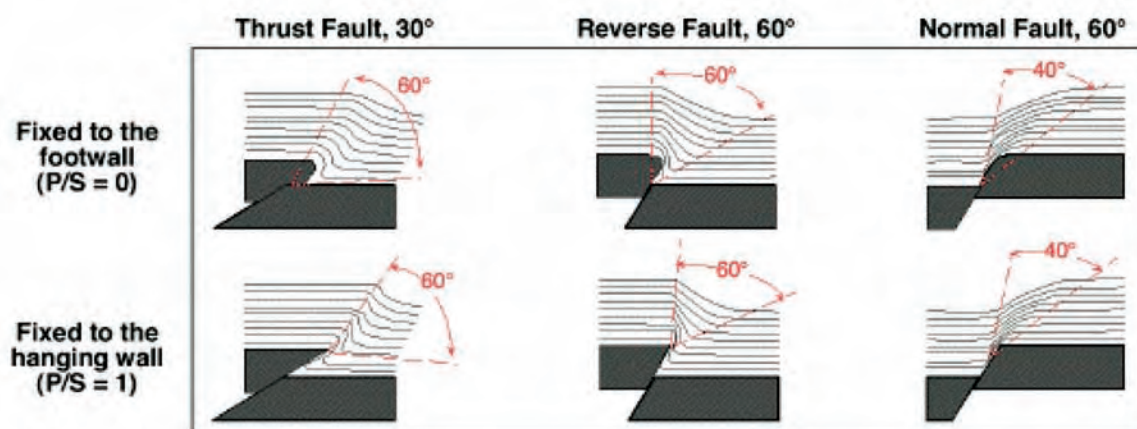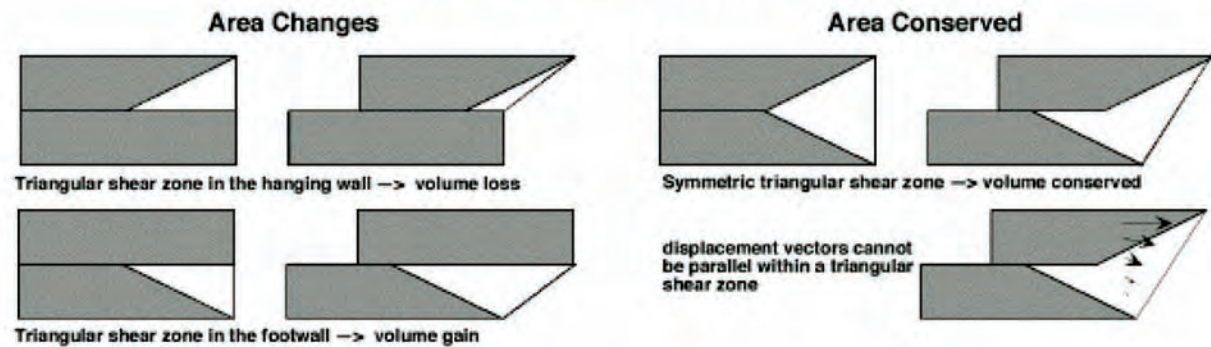
Fig. 47 - The trishear model (ERSLEV, 1991, ALLMENDINGER, 1998) explains most of the deformation occurring at the tip line of faults.

http://www.geo.cornell.edu/RWA/trishear/default.html

The Trishear concept of Erslev (1991)

Area Changes

Triangular shear zone in the hanging wall —> volume loss

Triangular shear zone in the footwall —> volume gain

Area Conserved

Symmetric triangular shear zone —> volume conserved

displacement vectors cannot be parallel within a triangular shear zone

	Thrust Fault, 30°	Reverse Fault, 60°	Normal Fault, 60°
Fixed to the footwall (P/S = 0)	60°	60°	40°
Fixed to the hanging wall (P/S = 1)	60°	60°	40°

Growth Triangles in Trishear Fault-propagation Folds
Allmendinger (1998)

growth axial surface

growth strata

Active Axis

migration of hanging wall boundary through the rock

Fixed Axis—initial position of hanging wall trishear boundary along these material points

P/S = 2.0

R. Allmendinger © 1999
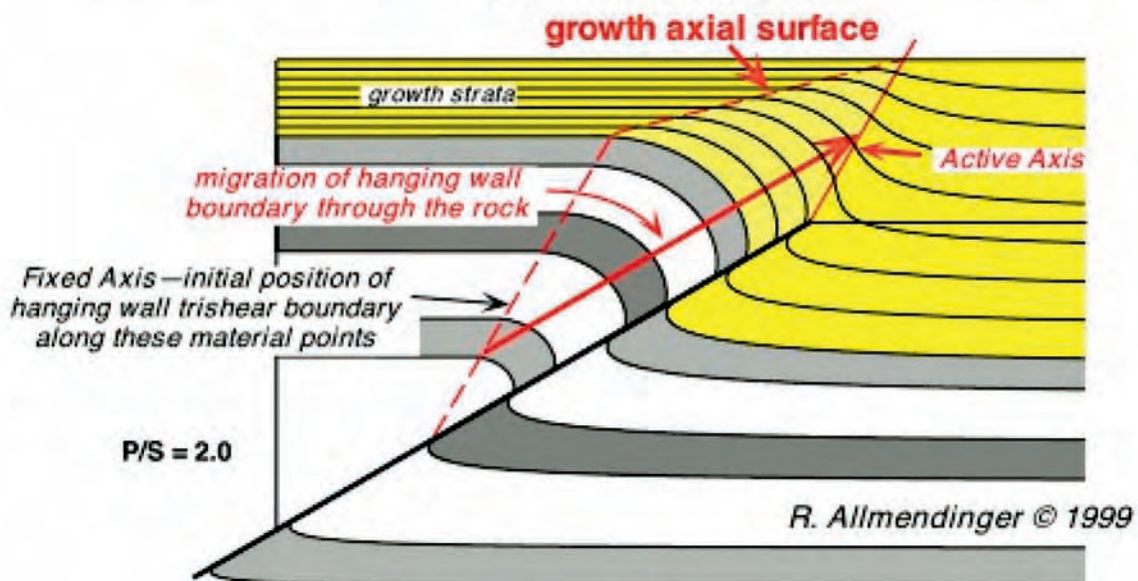
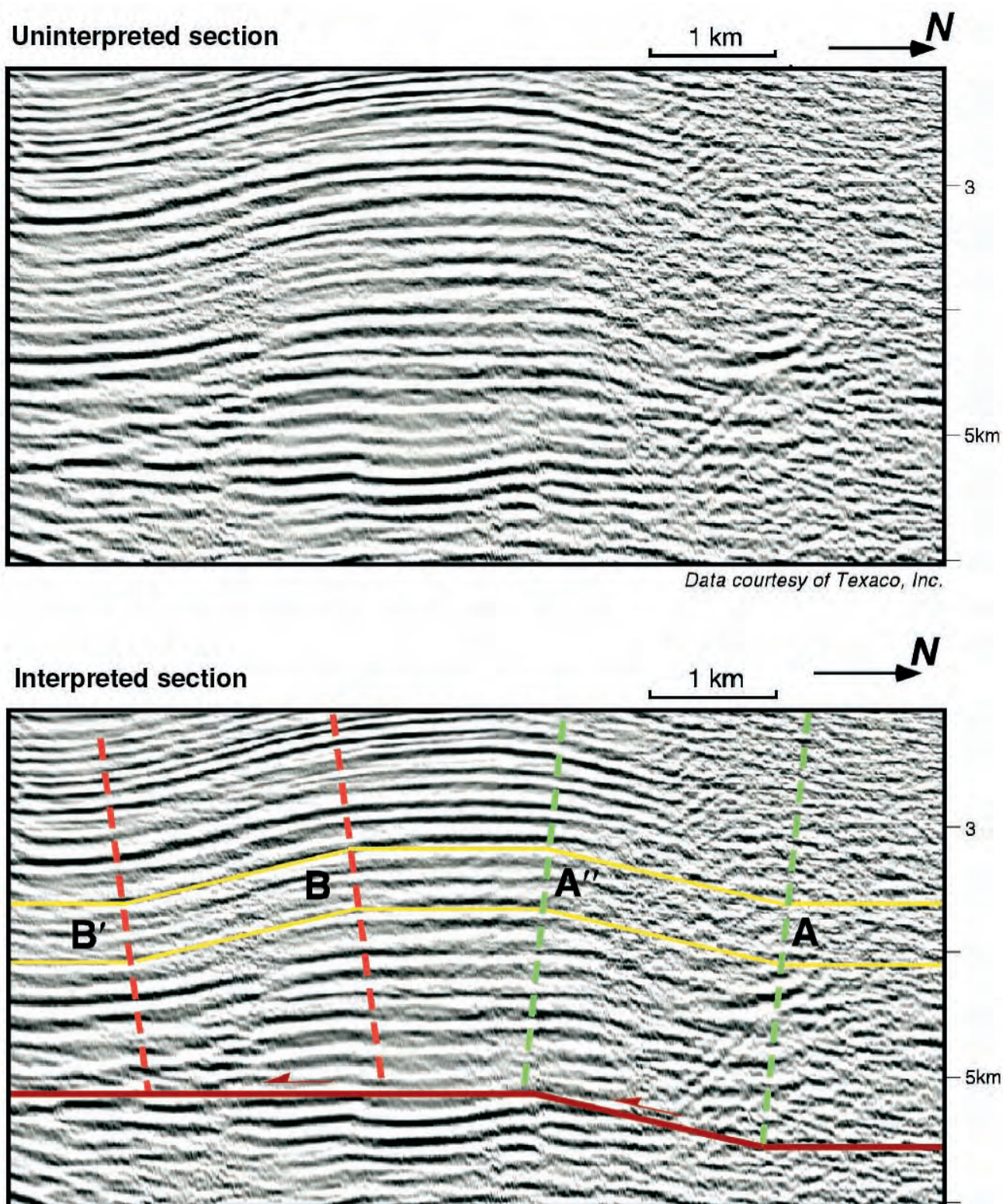Fig. 48 - The trishear concept as expressed by ERSLEV (1991) and ALLMENDINGER (1998).

Fig. 49 - Seismic section of a fault bend fold. Pitas Point, Santa Barbara Channel, California, USA. After SHAW *et alii* (2005) AAPG©, reprinted by permission of the AAPG whose permission is required for further use.
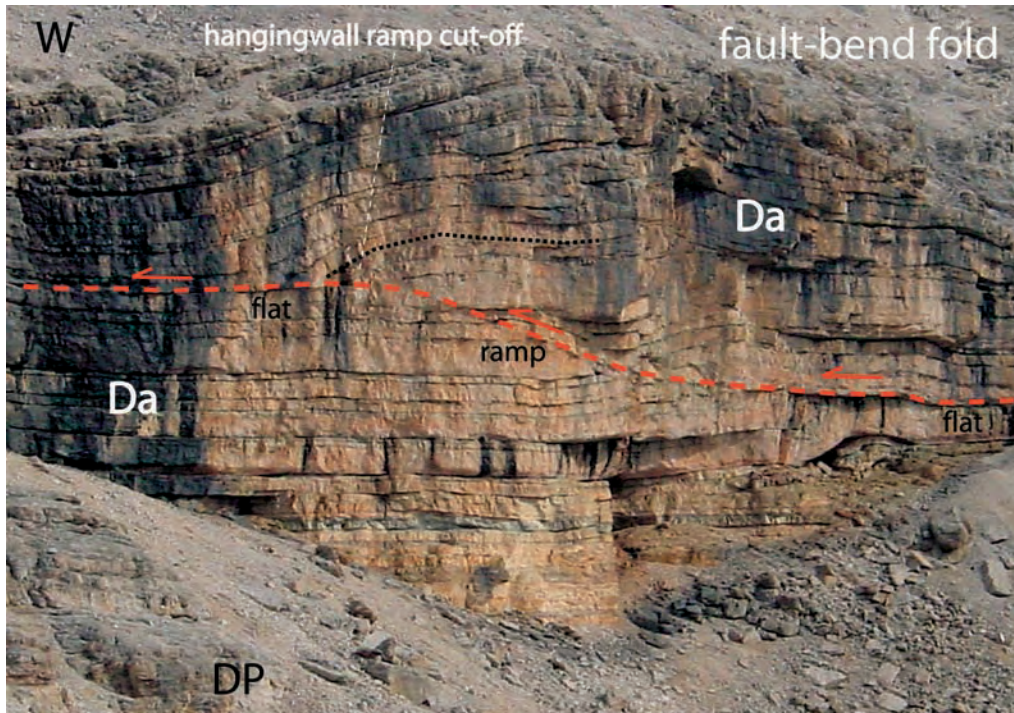
Fig. 50 - Fault-bend fold in the Dachstein Limestone (Da) of the southern cliff of the Piz Boè, Sella Massif, Dolomites. Note the fore-limb inclined toward the vergence. Dolomia Principale (DP). The cliff is about 20 m high.
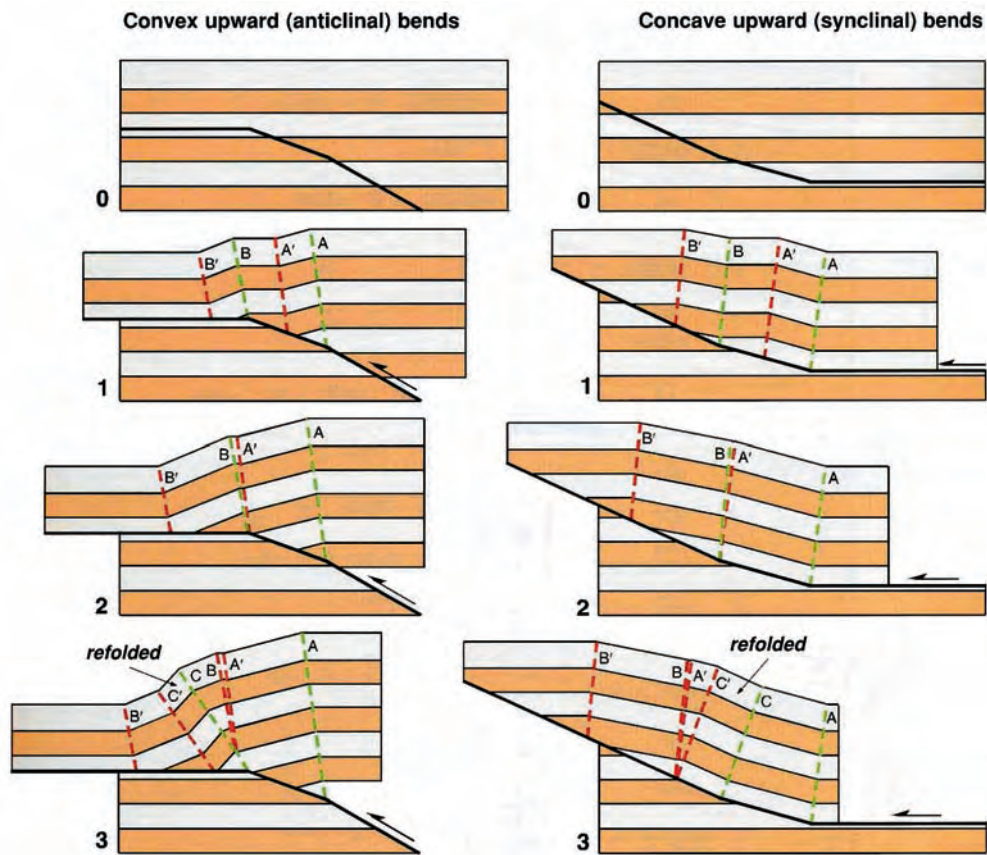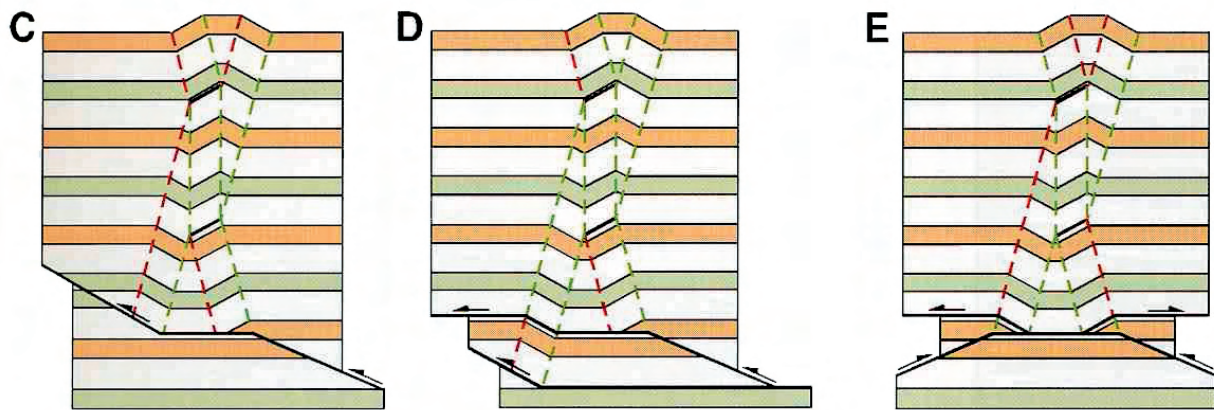

Fig. 51 - Fault trajectories may be characterised by two or more bends with the same concavity or convexity. These features produce multi-bend fault-bend folds. After SHAW *et alii* (2005) AAPG©, reprinted by permission of the AAPG whose permission is required for further use.

Fig. 52 - Fold interference structures form when two or more fault-bend kink bends intersect. This produces for example anticlines over synclines. After SHAW *et alii* (2005) AAPG©, reprinted by permission of the AAPG whose permission is required for further use.
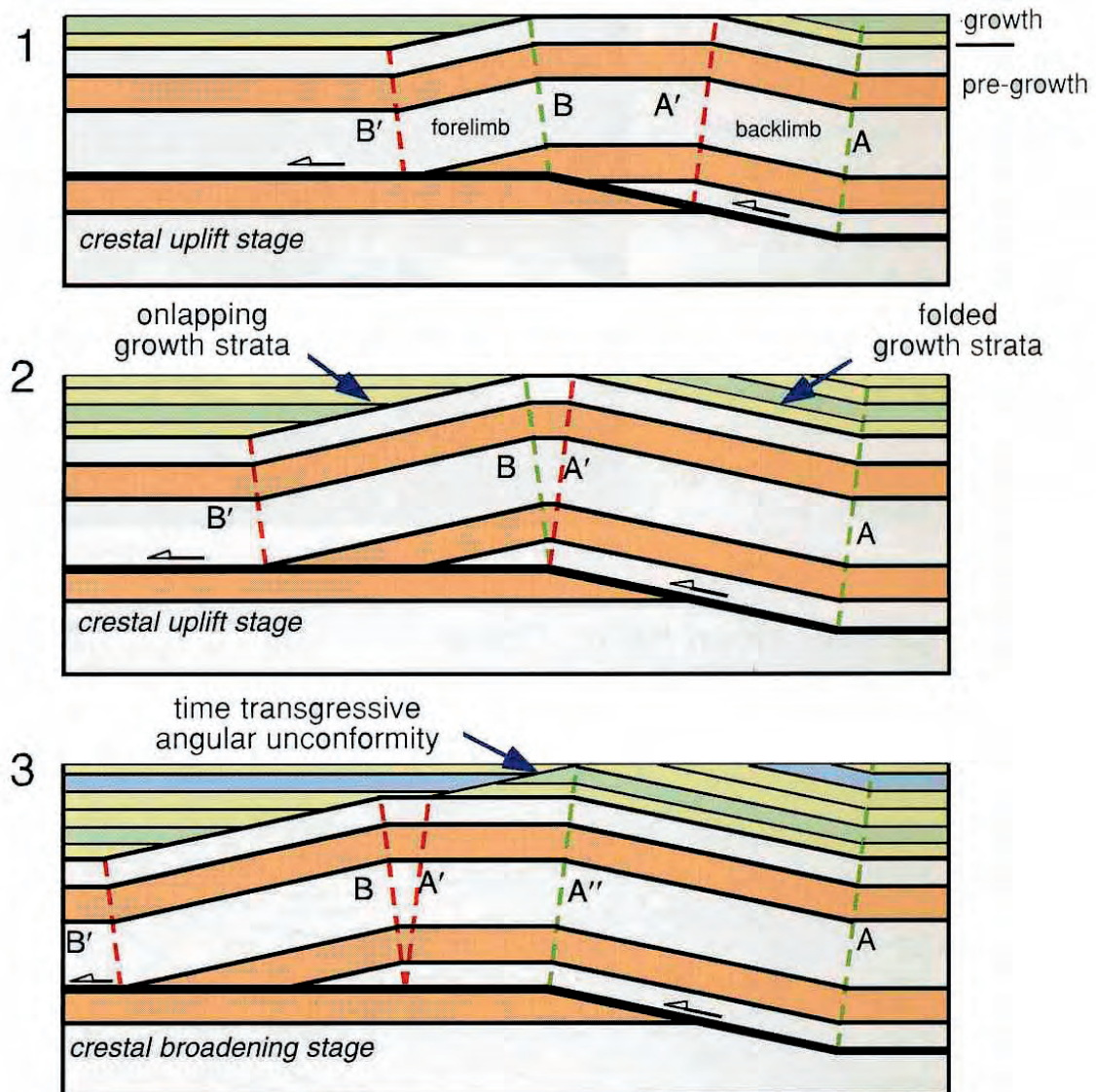

Fig. 53 - Growth-fold associated to fault bending with low sedimentation rates (i.e., sedimentation rates slower or equal to uplift rates). After SHAW *et alii* (2005) AAPG©, reprinted by permission of the AAPG whose permission is required for further use.
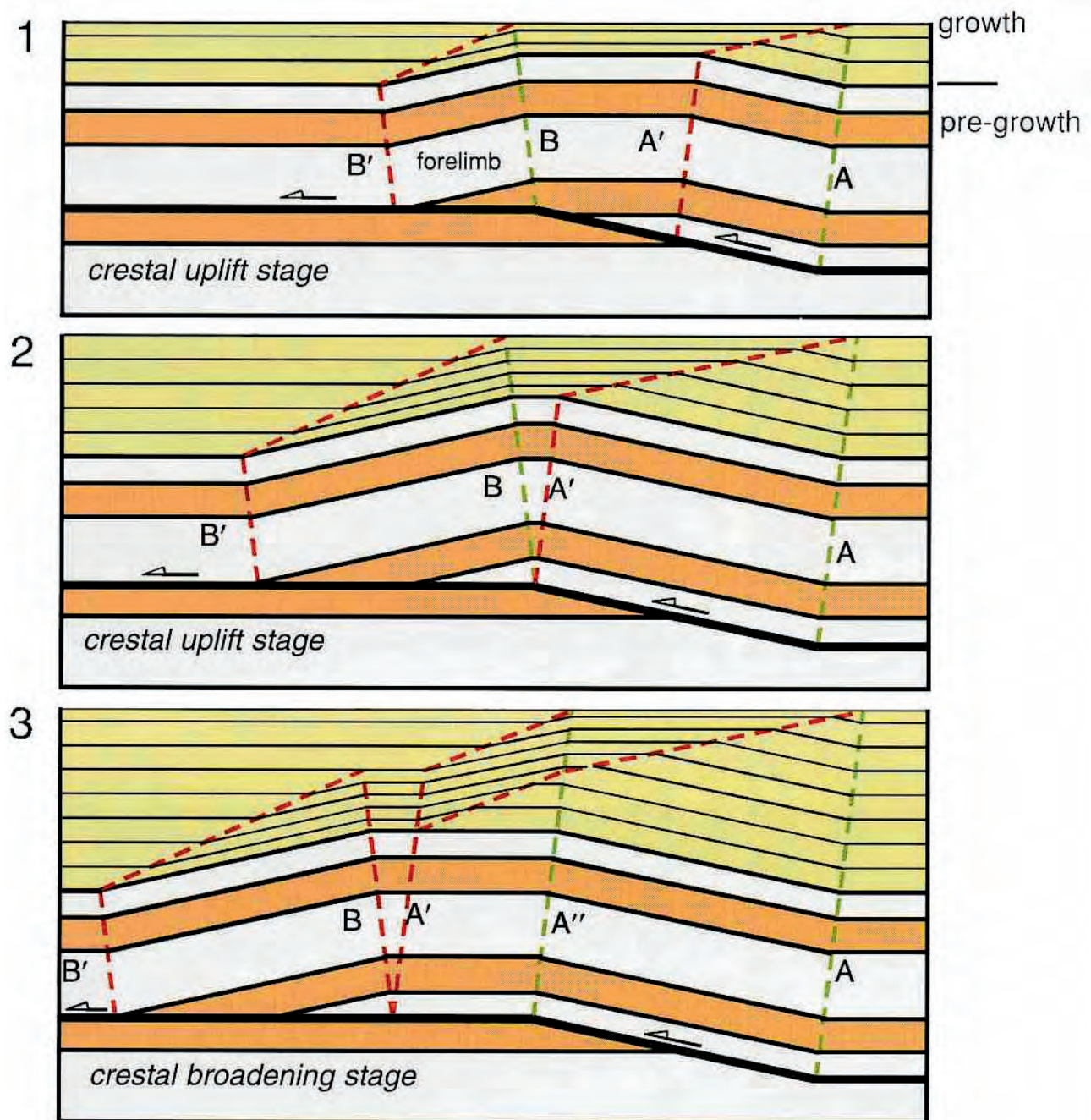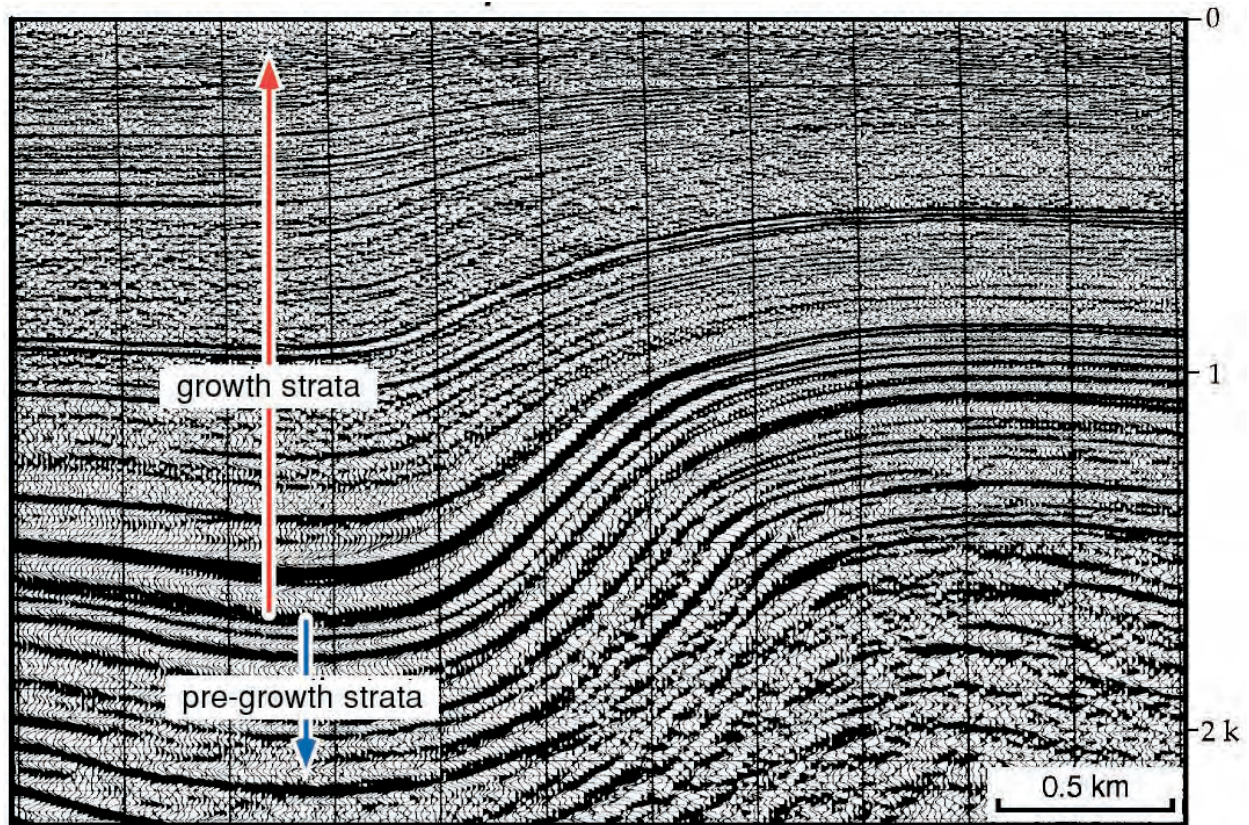
Fig. 54 - Growth fold associated to fault bending with high sedimentation rates (i.e., sedimentation rates faster than uplift rates). After SHAW *et alii* (2005) AAPG©, reprinted by permission of the AAPG whose permission is required for further use.

Data courtesy of Caltex and Texaco, Inc.

Fig. 55 - Growth fold characterised by sedimentation exceeding uplift. Notice that the growth strata, bounded by two seismic reflections, thin towards the structural high. After Sнaw *et alii* (2005) AAPG©, reprinted by permission of the AAPG whose permission is required for further use.
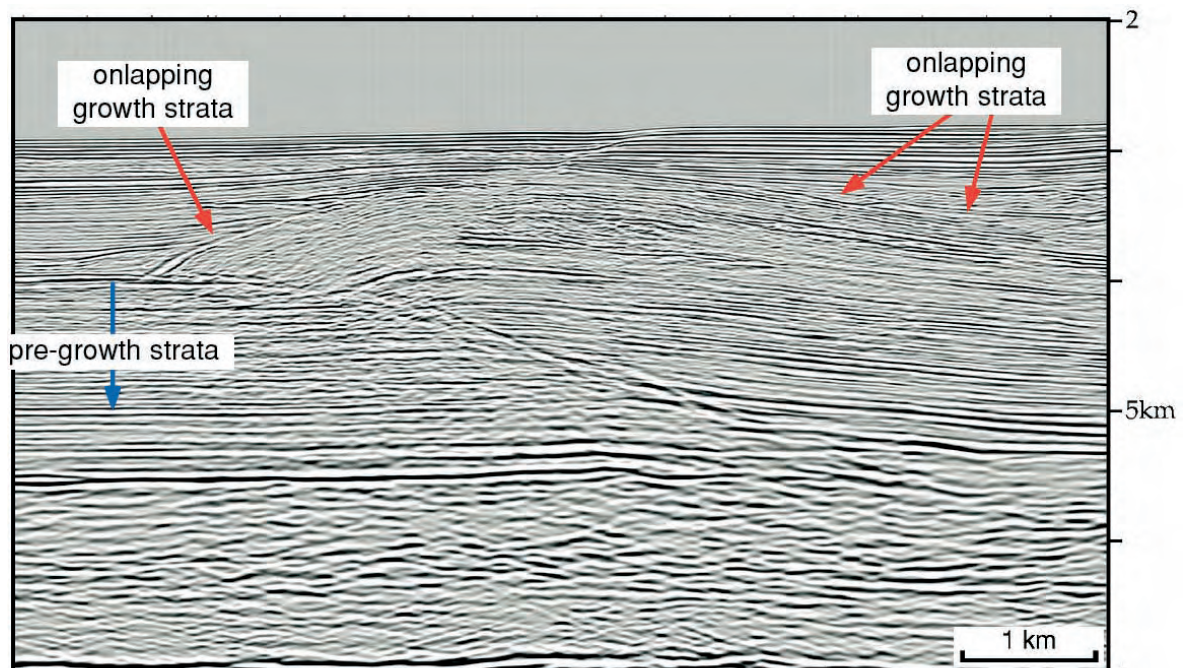
Data courtesy of VERITAS DGC Limited

Fig. 56 - Growth fold characterised by uplift exceeding sedimentation. Growth-strata typically thin toward and onlap the structural high. Growth strata do not occur on the crest of the anticline. After Sнaw *et alii* (2005) AAPG©, reprinted by permission of the AAPG whose permission is required for further use.
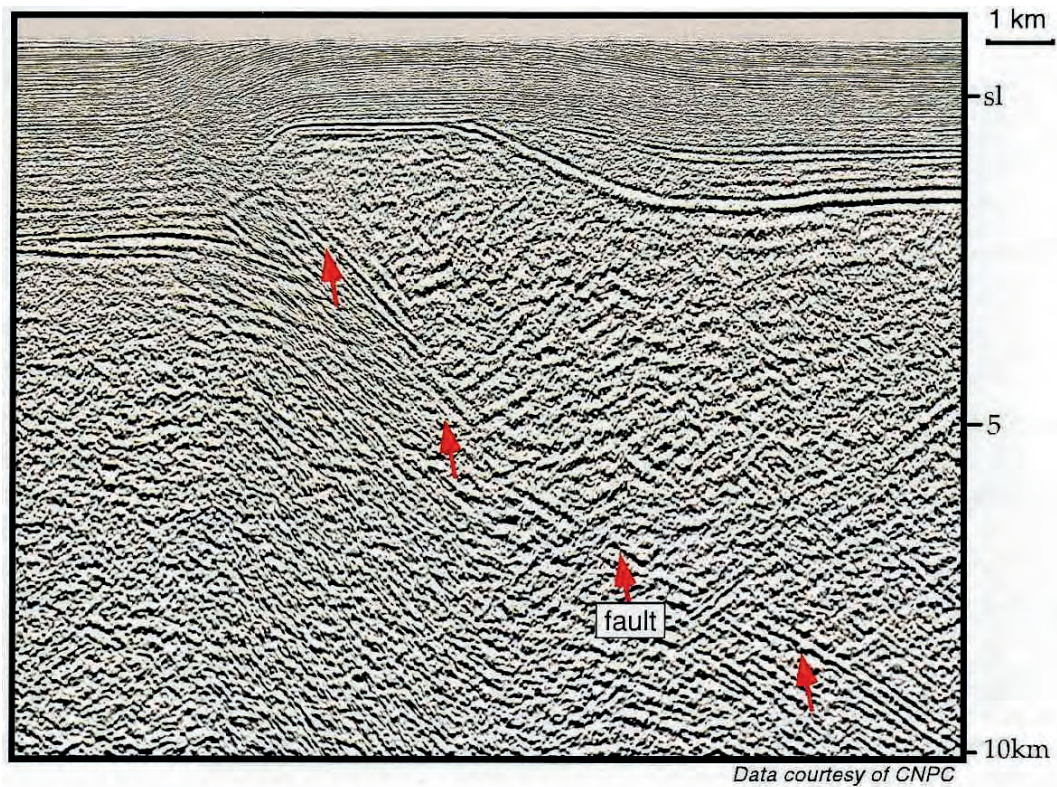
Fig. 57 - Seismic section through a fault-propagation fold in the Tarim Basin, China. After SHAW *et alii* (2005) AAPG©, reprinted by permission of the AAPG whose permission is required for further use.

Fig. 58 - Fault-propagation fold, southeastern cliff of Col Bechei, Dolomites. This type of structure is the most common for brittle regime in the orogens worldwide.
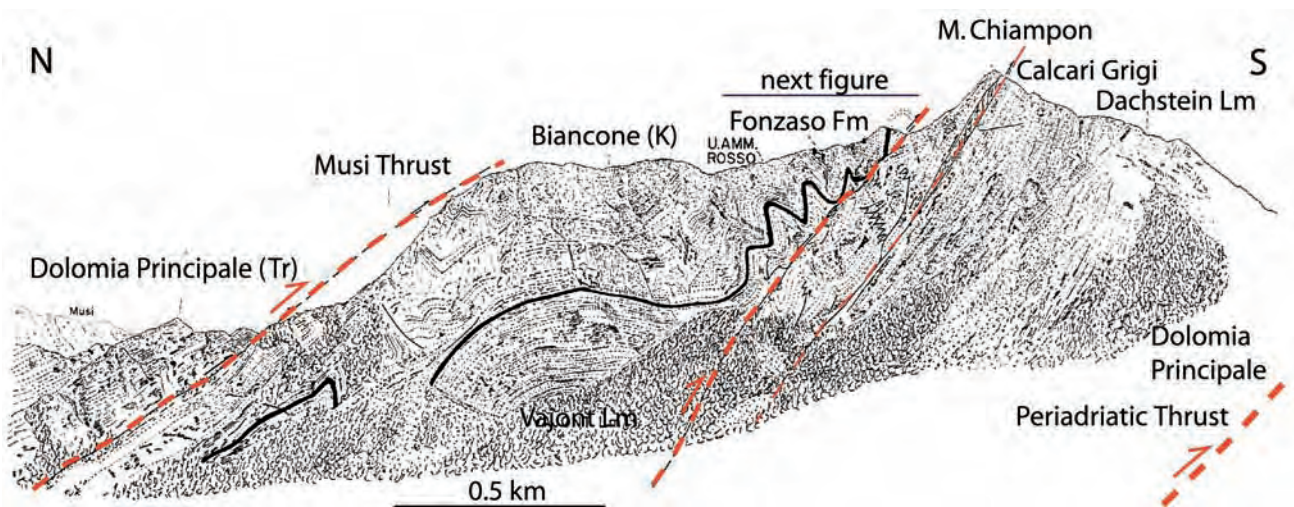
Fig. 59 - Natural section of the Mt. Chiampon, near Venzone, Friuli, eastern Southern Alps. Two major thrusts (Musi Thrust, eastward prolongation of the Valsugana Thrust, and Periadriatic Thrust) contain an intervening folded and internally sheared slice of Mesozoic rocks (platform facies up to Liassic, and deep water up to the Cretaceous).
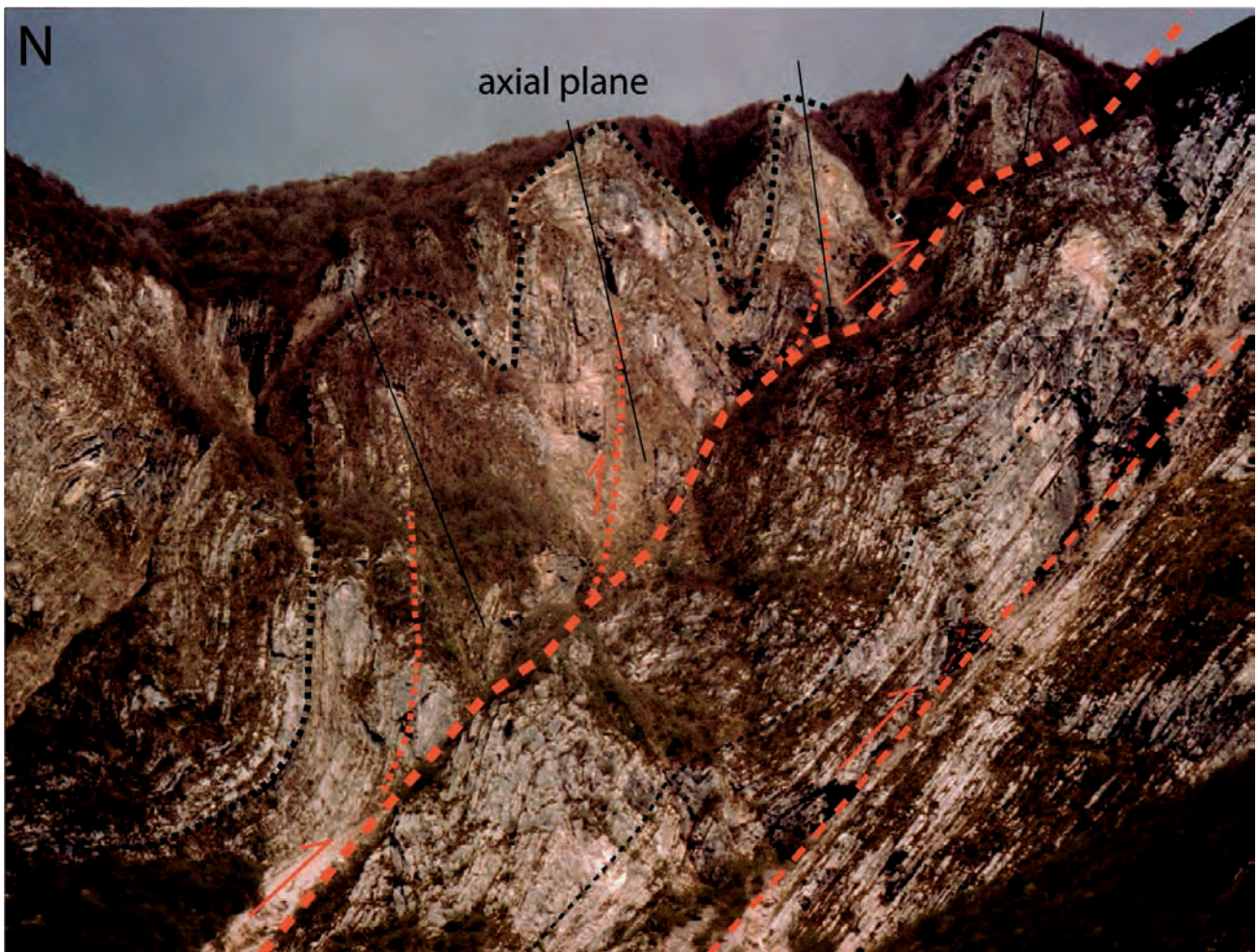

Fig. 60 - Detail of the previous figure. The upper decollement is older and has been tilted and folded by the deeper decollements. Note the gradual counter-clockwise rotation of the axial planes of the detached folds due to piggy back forward propagation of the imbricate fan.
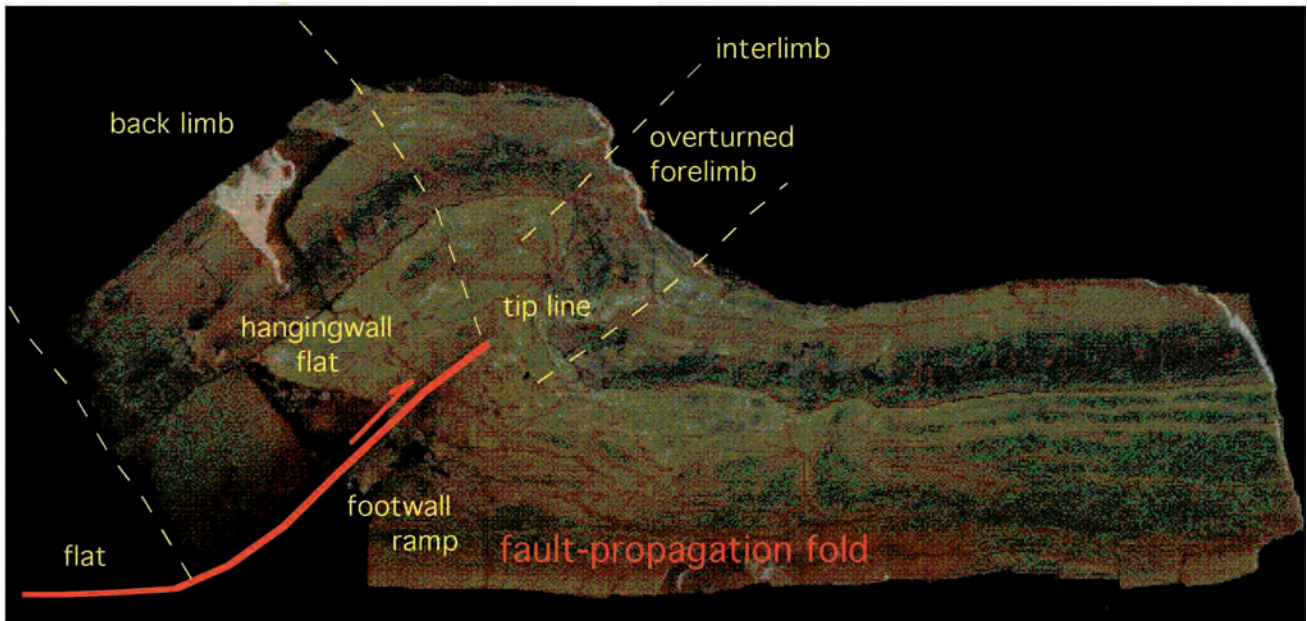
Fig. 61 - Fault-propagation fold in a 25 cm wide specimen of the Lagonegro Jurassic Scisti Silicei, Southern Apennines. Notice the transfer of shortening from the thrust to the fold. Unlike the fault-bend fold mechanism, the forelimb tends to be vertical or overturned. The backlimb has the inclination of the ramp.
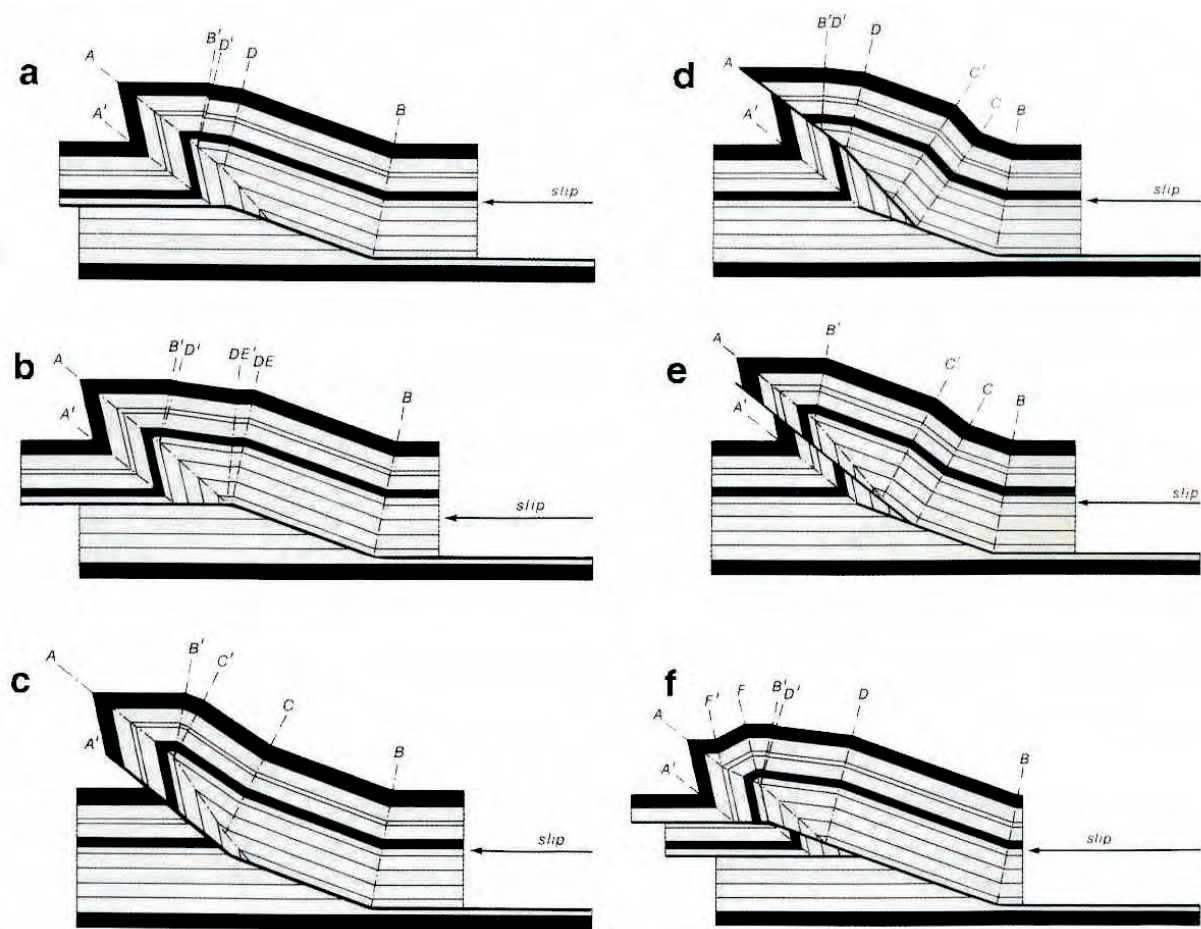

Fig. 62 - Cartoon showing the possible breakthrough structures associated to fault-propagations folds. a) and b) decollement breakthrough; c) synclinal breakthrough; d) anticlinal breakthrough; e) high-angle-forelimb breakthrough; f) low-angle breakthrough. After SHAW *et alii* (2005) AAPG©, reprinted by permission of the AAPG whose permission is required for further use.
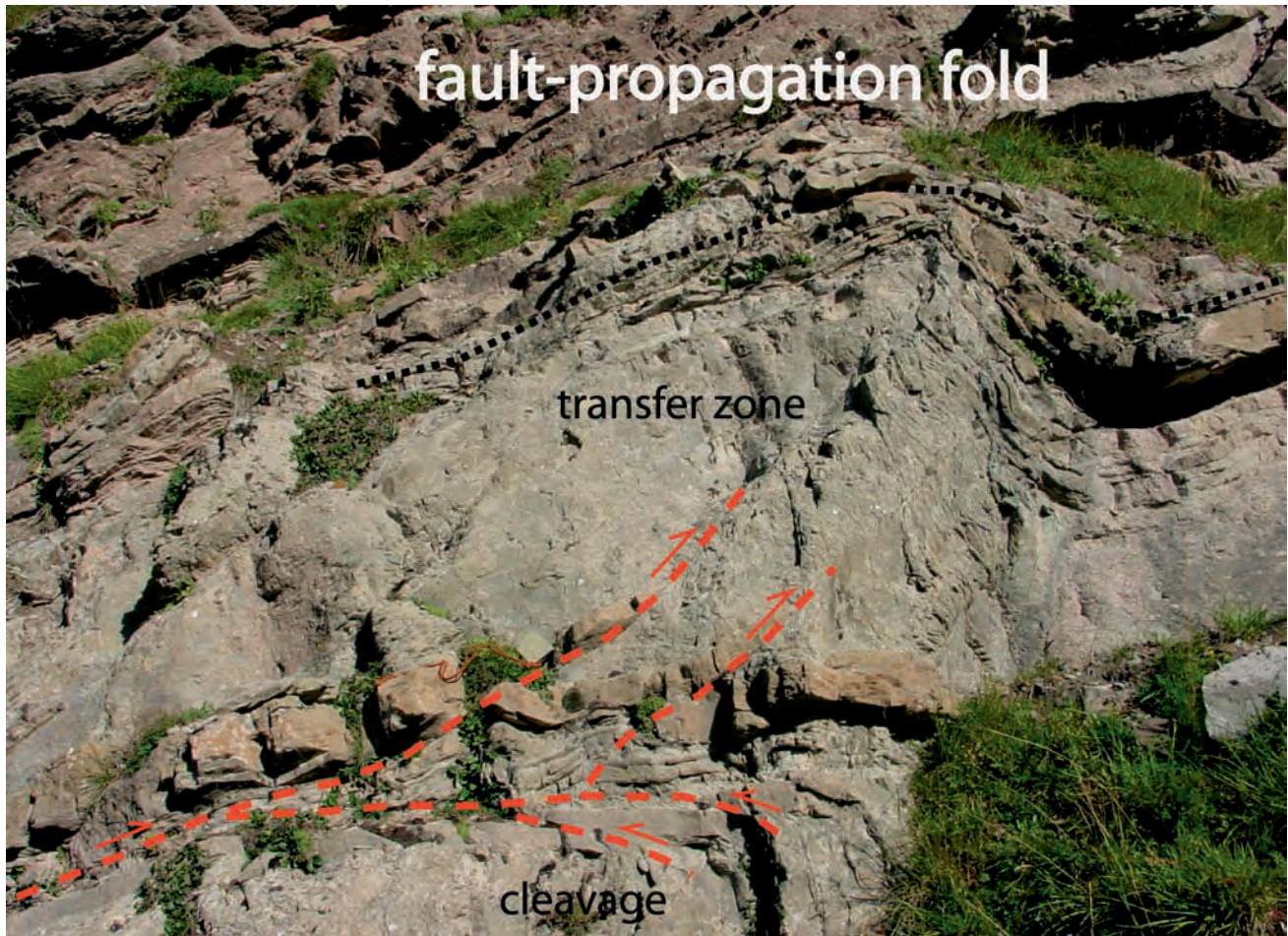
Fig. 63 - Fault-propagation fold in the Siusi Member, within the olistholith of Werfen Fm at Varda (Dolomites). Note the partitioning of the strain associated to the shortening. In the transfer zone thrusting gradually decreases and passes into folding. In the lower part, small backthrusts disappear at depth into vertical slaty cleavage accommodating the shortening.
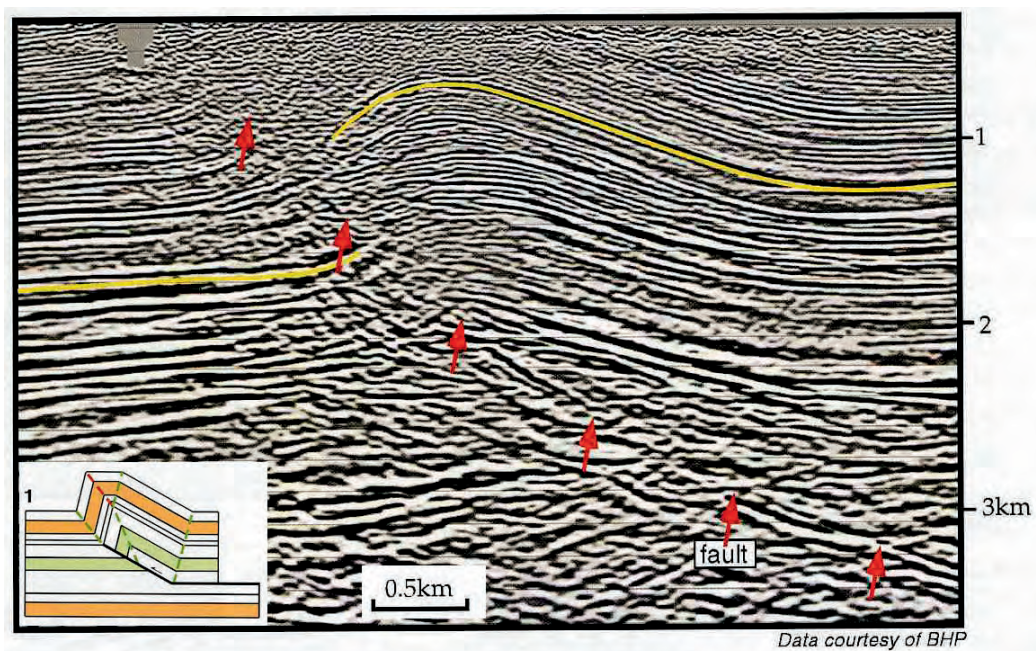

Fig. 64 - Seismic section showing a forelimb breakthrough pattern. After SHAW *et alii* (2005) AAPG©, reprinted by permission of the AAPG whose permission is required for further use.

Fig. 65 - Fault-propagation fold at the hinge of a chevron fold in the Ladinian basinal Livinallongo Fm. 1 km west of Livinallongo del Col di Lana, Dolomites.

Fig. 66 - Tight syncline in Tertiary flysch, Castiglioncello, Tuscany. Note the hinge thickening of shales, whereas the sandstone beds maintain their thickness.
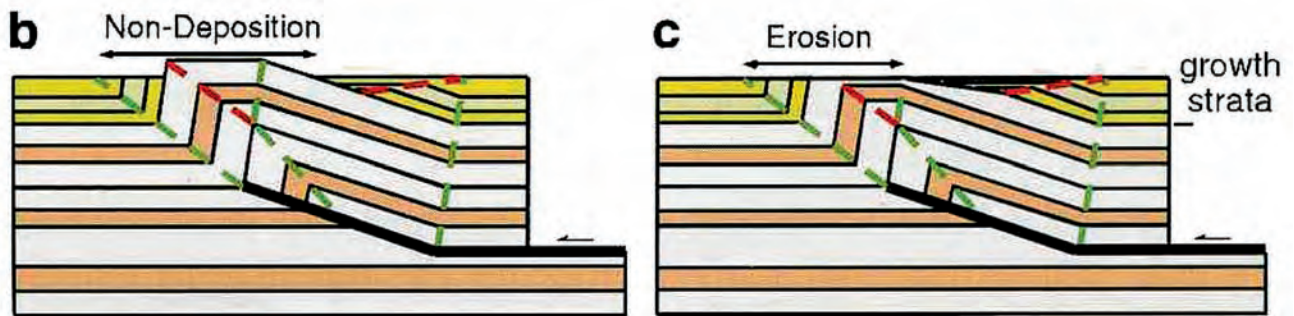
Fig. 67 - Growth fault-propagation folding with sedimentation rates slower than uplift rates. Notice that in submarine conditions the crest of the growing anticline may be characterised by non-deposition, wherear it may be eroded in subaerial conditions. After SHAW *et alii* (2005) AAPG©, reprinted by permission of the AAPG whose permission is required for further use.
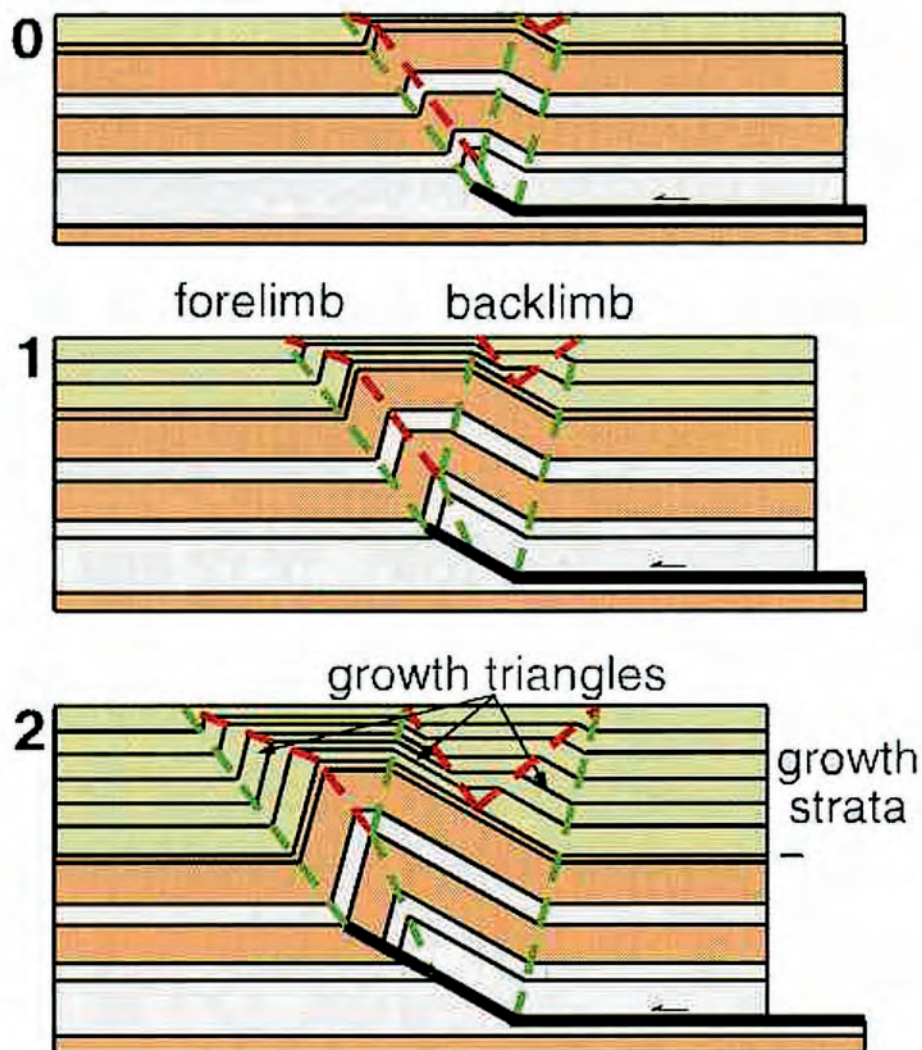

Fig. 68 - Growth fault-propagation folding with sedimentation rates greater than uplift rates. After SHAW *et alii* (2005) AAPG©, reprinted by permission of the AAPG whose permission is required for further use.

Fig. 69 - Growth fault-propagation fold in Pleistocene conglomerates. Alianello, Southern Apennines. Notice the thinning of syn-tectonic sediments toward the crest of the anticline.
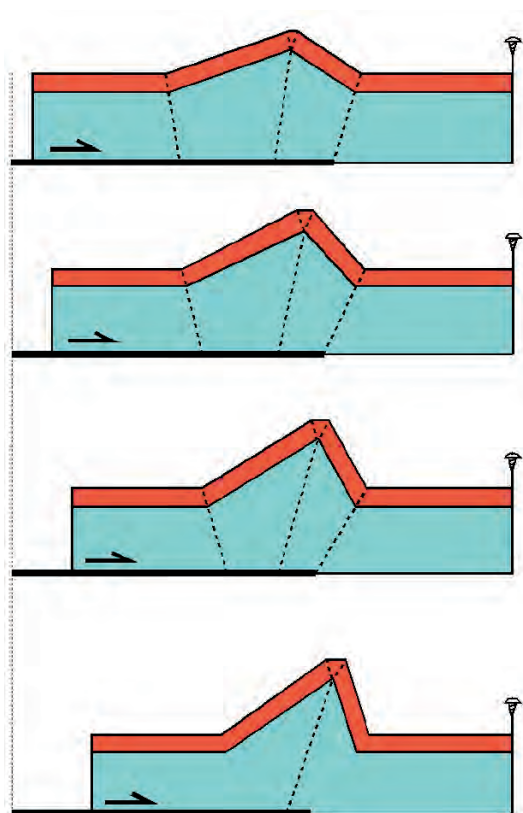

Fig. 70 - Detachment or decollement folds are generated above the tip line of a thrust that developed along a bedding-parallel detach-ment surface (i.e., along a flat). Where the thrust displacement dies to zero, the deformation is accommodated by folding in the hanging-wall. Modified after SHAW *et alii* (2005). AAPG©, reprinted by per-mission of the AAPG whose permission is required for further use.
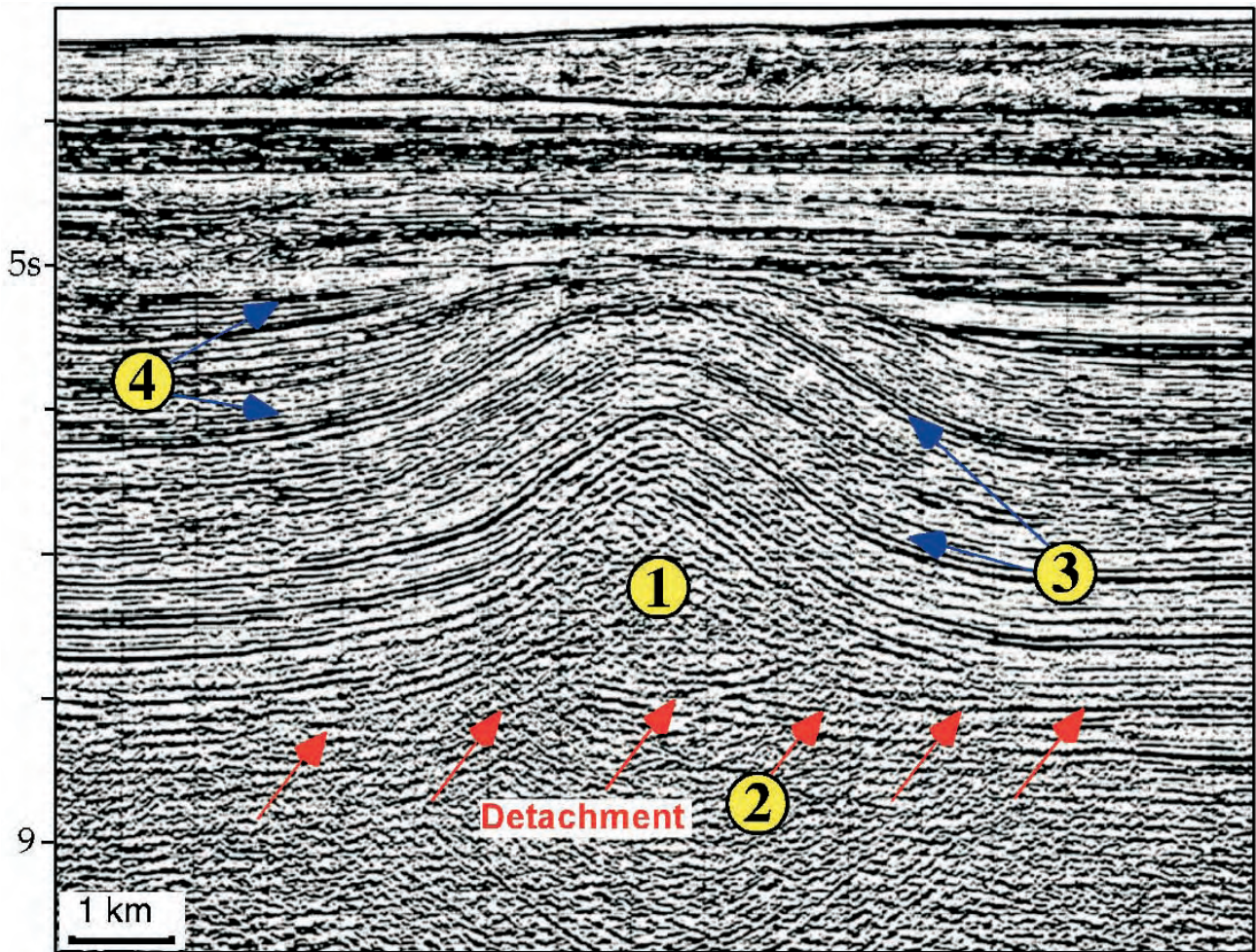
Fig. 71 - Seismic line of a detachment fold in the Gulf of Mexico. After SHAW *et alii* (2005) AAPG©, reprinted by permission of the AAPG whose permission is required for further use.

Fig. 72 - Detachment fold cropping out in the Opal Mt., Canadian Rocky Mountains. Modified after BONS, 2007 (http://homepages.uni-tuebingen.de/paul.bons/paul/lectures/structure/index.html).
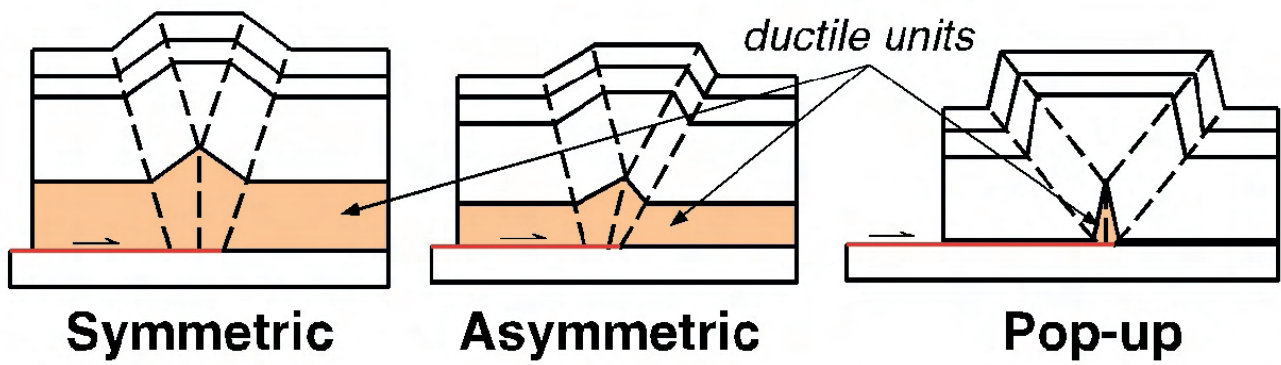
Fig. 73 - Possible geometries of detachment folds. After Shaw *et alii* (2005) AAPG©, reprinted by permission of the AAPG whose permission is required for further use.
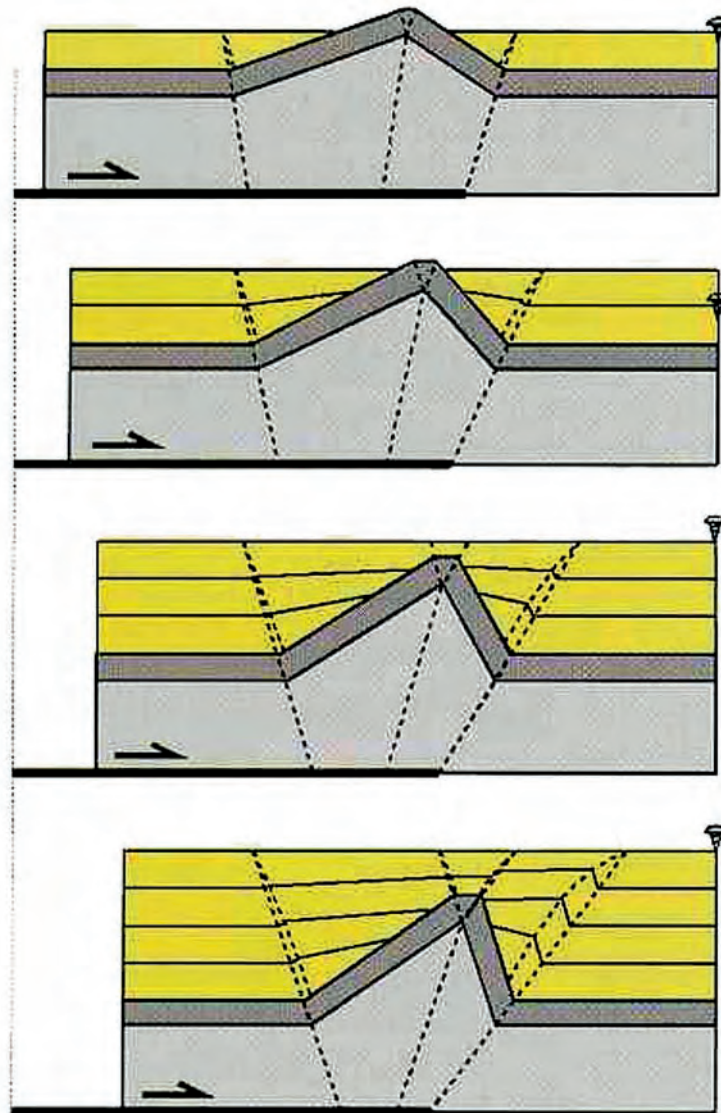

Fig. 74 - Models of growth detachment folds. Different ratios of sedimentation vs. uplift rates (increasing toward the bottom of the figure) are shown. After Shaw *et alii* (2005) AAPG©, reprinted by permission of the AAPG whose permission is required for further use.

Fig. 75 - Chevron folds in the Livinallongo Fm. Note the decoupling surface above where the thickness of the beds increase and the underlying tight folds disappear. The fold axis is NNW-trending. Gasoline station, Pieve di Livinallongo.
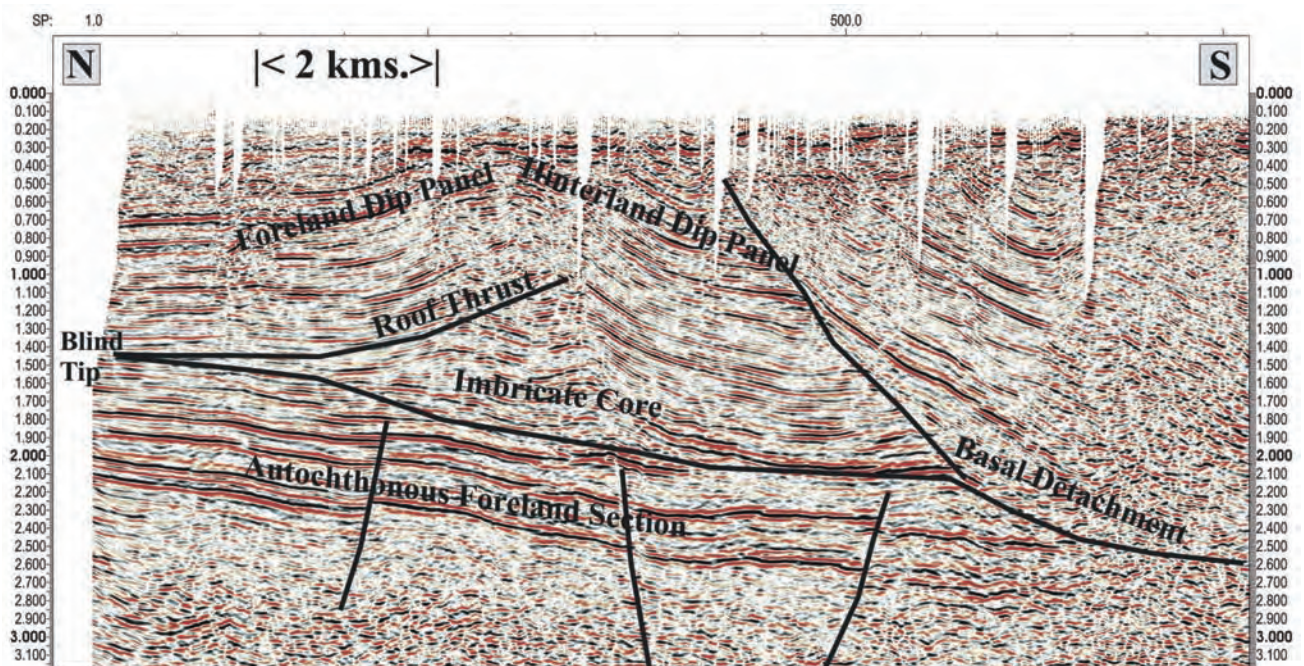

Fig. 76 - Example of triangle zone at the Alpine front in Bavaria (after BERGE & VEAL, 2005)

DECOLLEMENT DEPTH 2.5 km

200 km

30 km

Moho

500 km² accreted rocks -≈10% erosion

5 km

Moho

1000 km²

10 km

Moho

2000 km²

LID

20 km

Moho

4000 km²
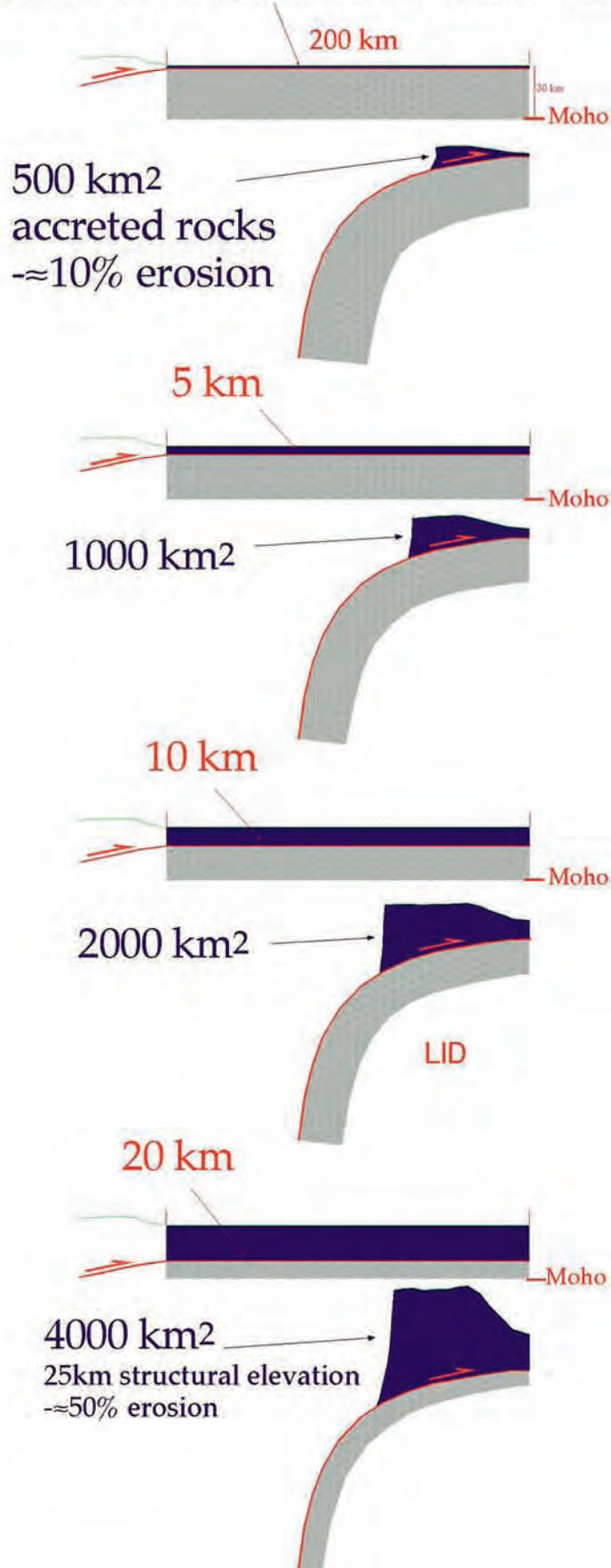25km structural elevation -≈50% erosion

Fig. 77 - The volumes involved by orogens and accretionary prisms are a function of the length of subduction and the depth of the basal decollement. Here are examples of an idealized subduction of 200 km and incremental depths of the decollement. As the decollement becomes deeper, the volume of the orogen will be larger, and its structural and morphologic elevation greater. In nature, the basal decollement is more undulating and shallower for west-directed subduction zones, which in fact present lower volumes in the hangingwall.
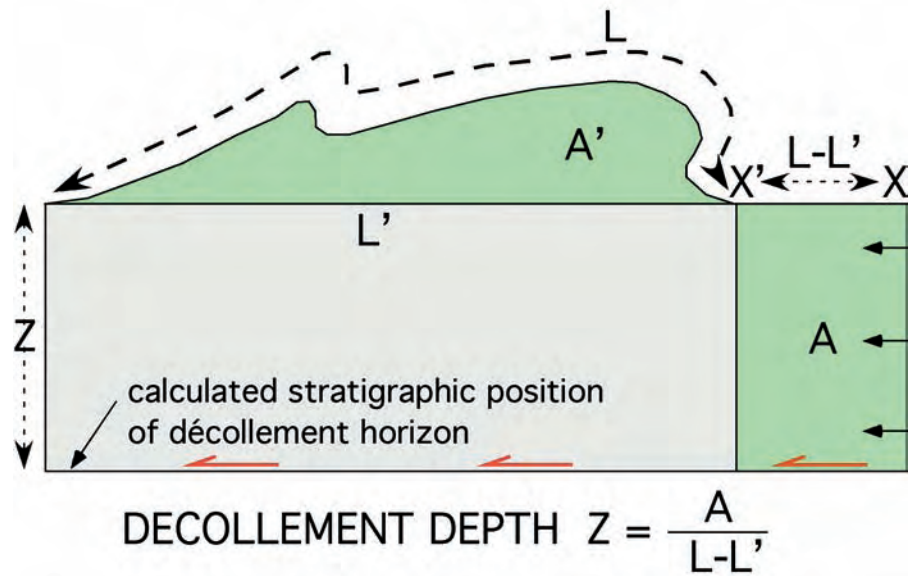
$$\text{DECOLLEMENT DEPTH } Z = \frac{A}{L-L'}$$

Fig. 78 - The décollement depth (Z) is the fundamental information for tectonic reconstructions. The depth can be estimated once the length of a marker bed (L) and the uplifted area (A) is measured. The uplifted area is equal to the shortened area. The area (A) divided by the difference between the original marker length (L) and the final shortened length (L') gives the calculated depth, after CHAMBERLIN, (1910) and MITRA & NAMSON (1989).
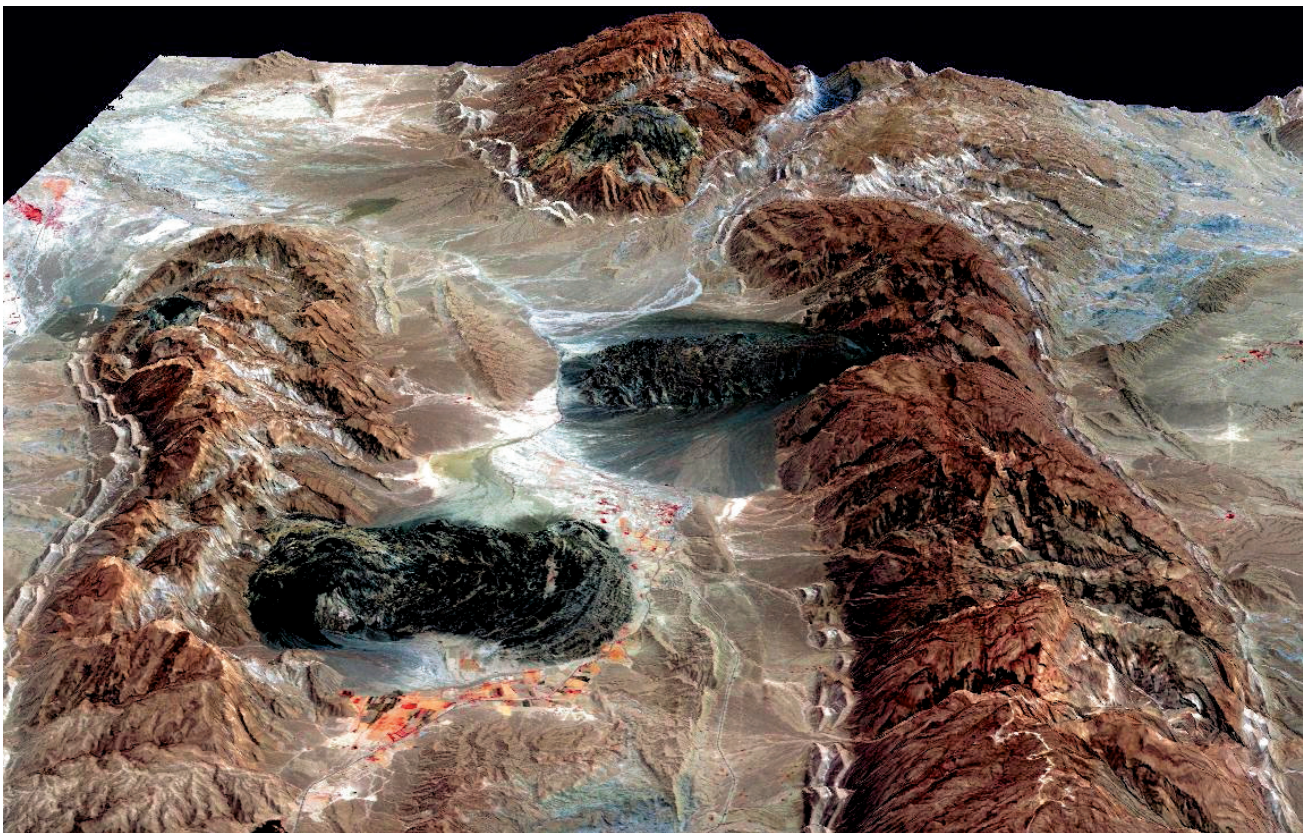

Fig. 79 - Folds in the Zagros. The large scale wavelength and amplitude of the folds indicate a deep decollement (10-14 km), which is located in early Paleozoic salt. Note three diapiric intrusions (darker rocks). USGS-Nasa picture.
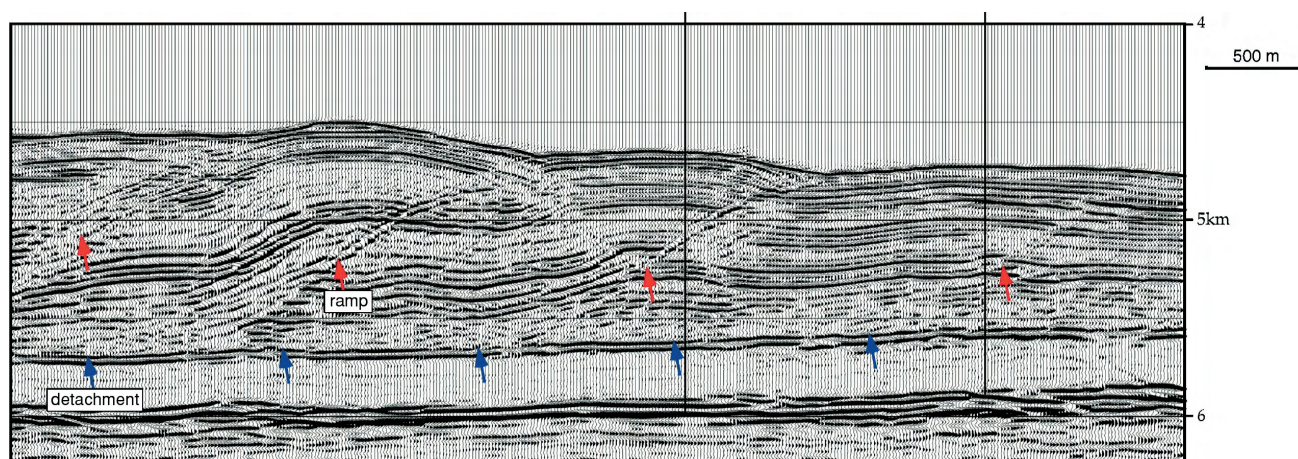
Fig. 80 - Seismic line through the Nankai Trough, Japan, showing the active front of the accretionary wedge associated to the Nankai subduction zone. Notice the ramps generating from a nearly subhorizontal basal decollement. Fault-bend folds accommodate the displacement along the ramp-flat thrust faults. After SHAW *et alii* (2005) AAPG©, reprinted by permission of the AAPG whose permission is required for further use.
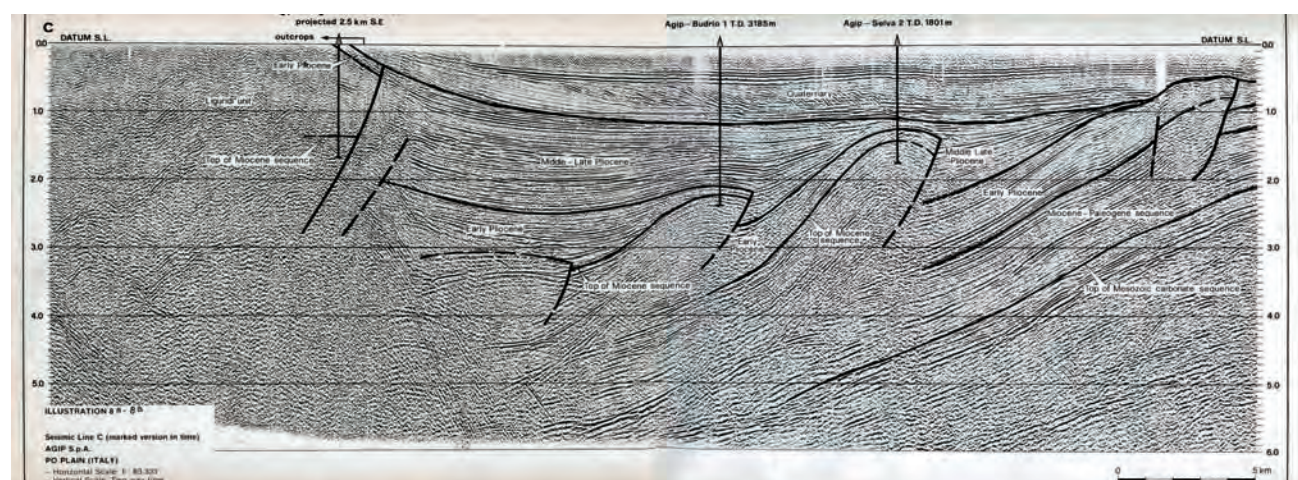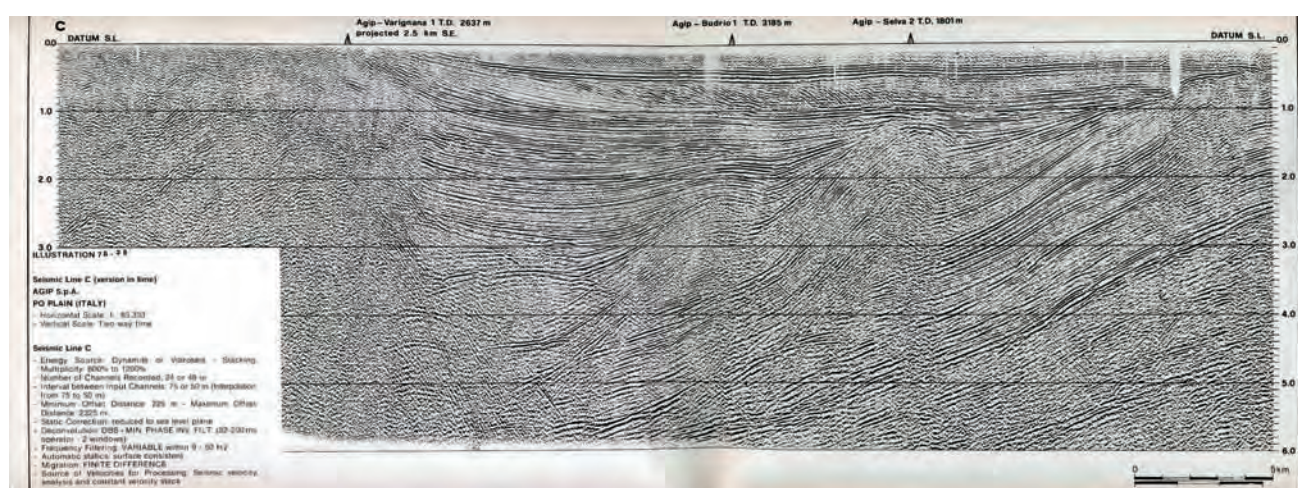

Fig. 81 - Seismic sections through the front of the Northern Apennines beneath the Po Plain. Notice that the two central growth fault-propagation folds are characterised by sedimentation faster than uplift (after PIERI, 1983).
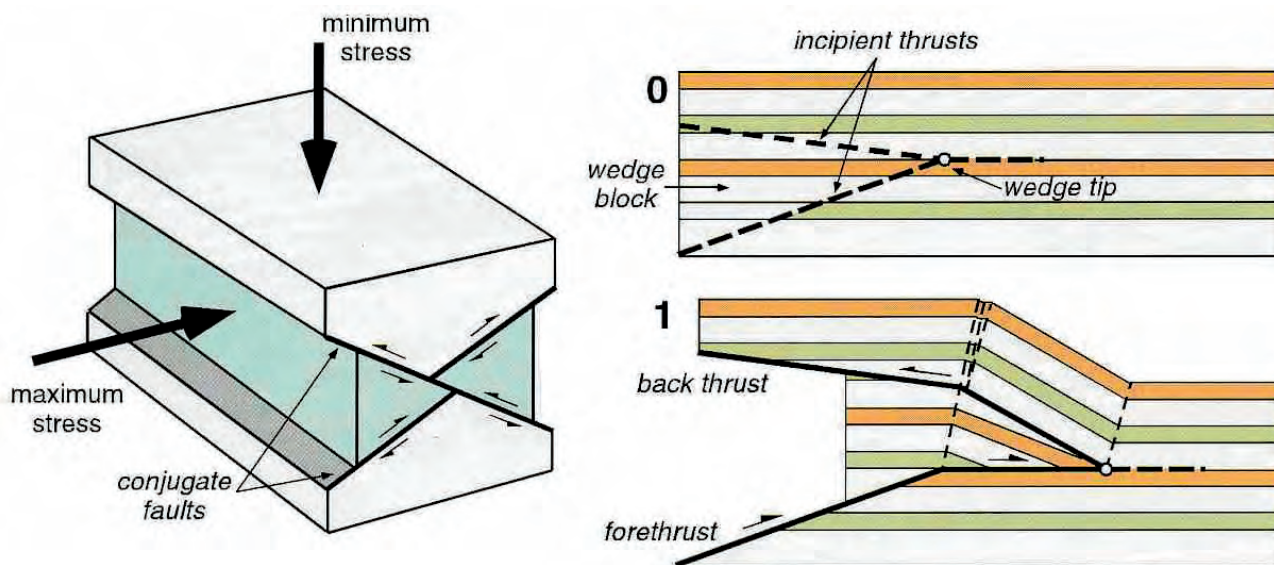
Fig. 82 - Structural wedges contain two connected fault segments that bound a triangular block. The two faults may be either two ramps or a ramp and a detachment. Structural wedges nucleate in agreement with the conjugate fault theory. Once nucleated, slip occurs along both faults allowing propagation of the wedge and determining the folding of the hangingwall. The lower thrust is named roof-thrust whereas the upper thrust is the back- (or roof-) thrust. At large scales wedges are referred to as triangle zones. After SHAW *et alii* (2005) AAPG©, reprinted by permission of the AAPG whose permission is required for further use.
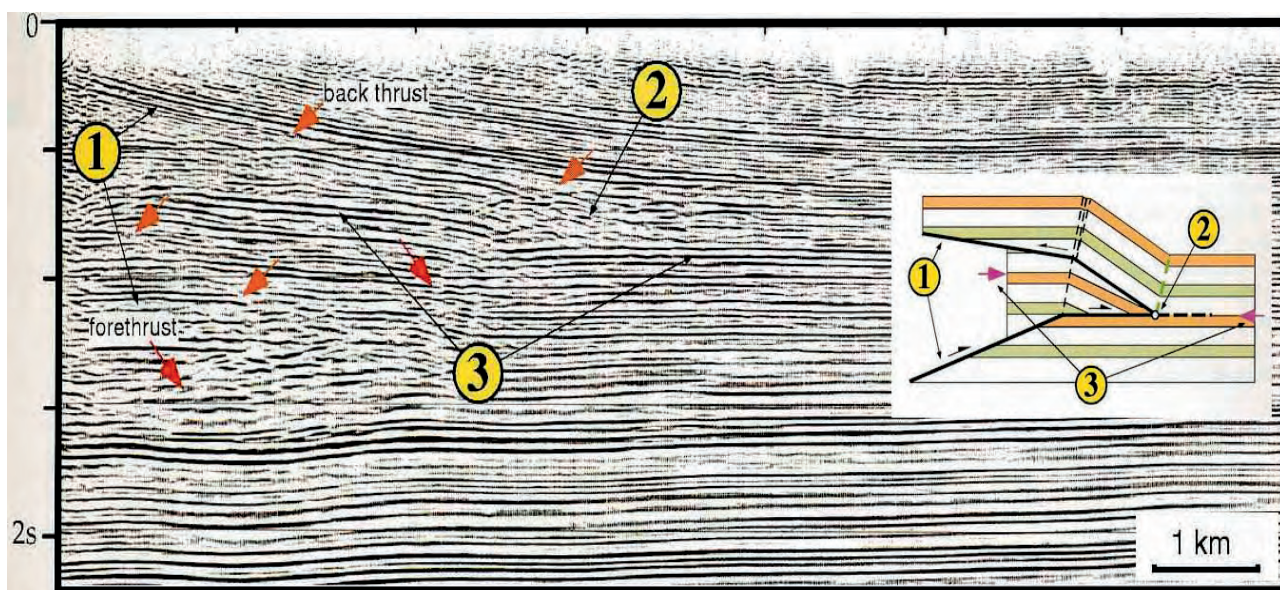

Fig. 83 - Seismic line showing a triangle zone imaged in the Alberta Foothills, Canada. The various structures highlighted by numbers are interpreted in the inset. After SHAW *et alii* (2005) AAPG©, reprinted by permission of the AAPG whose permission is required for further use.

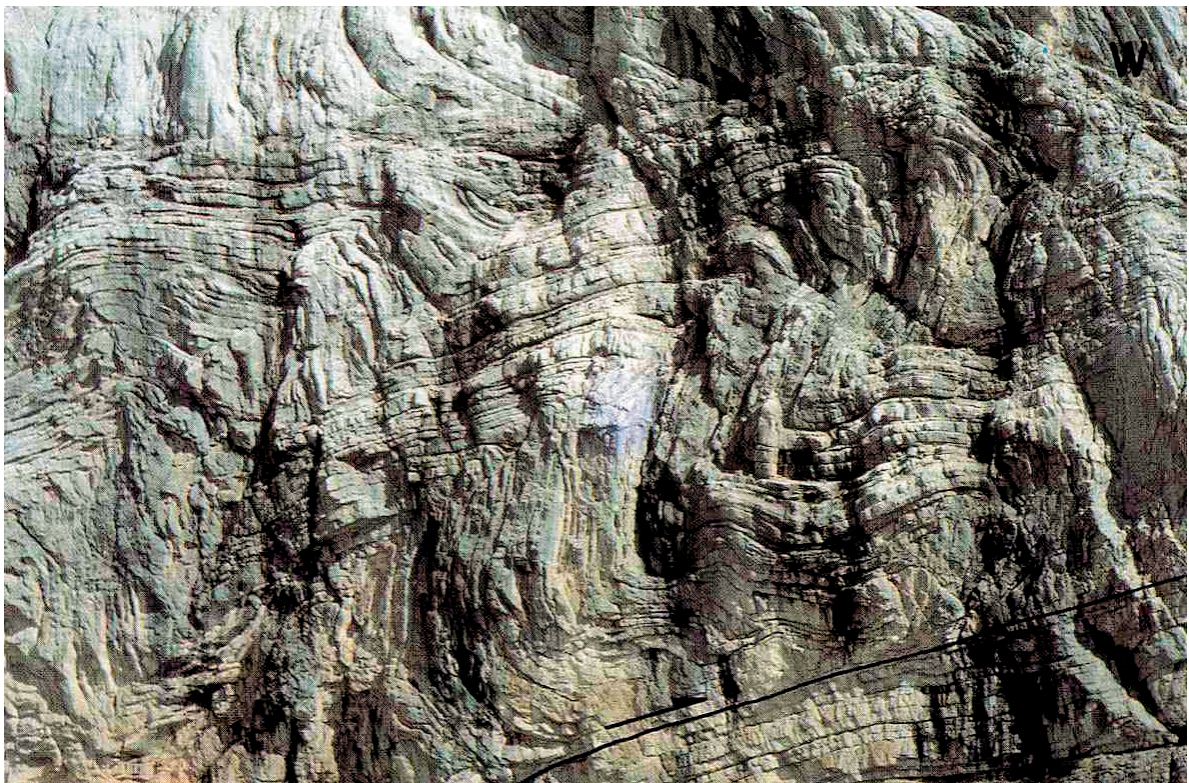Fig. 84 - Triangle zone in the Liassic Calcari Grigi, Tofana II, Dolomites. The outcrop is about 20 m wide.

Fig. 85 - WSW-verging chevron folds in Liassic Calcari Grigi in the hangingwall of the basal thrust of the Civetta klippe, Dolomites.
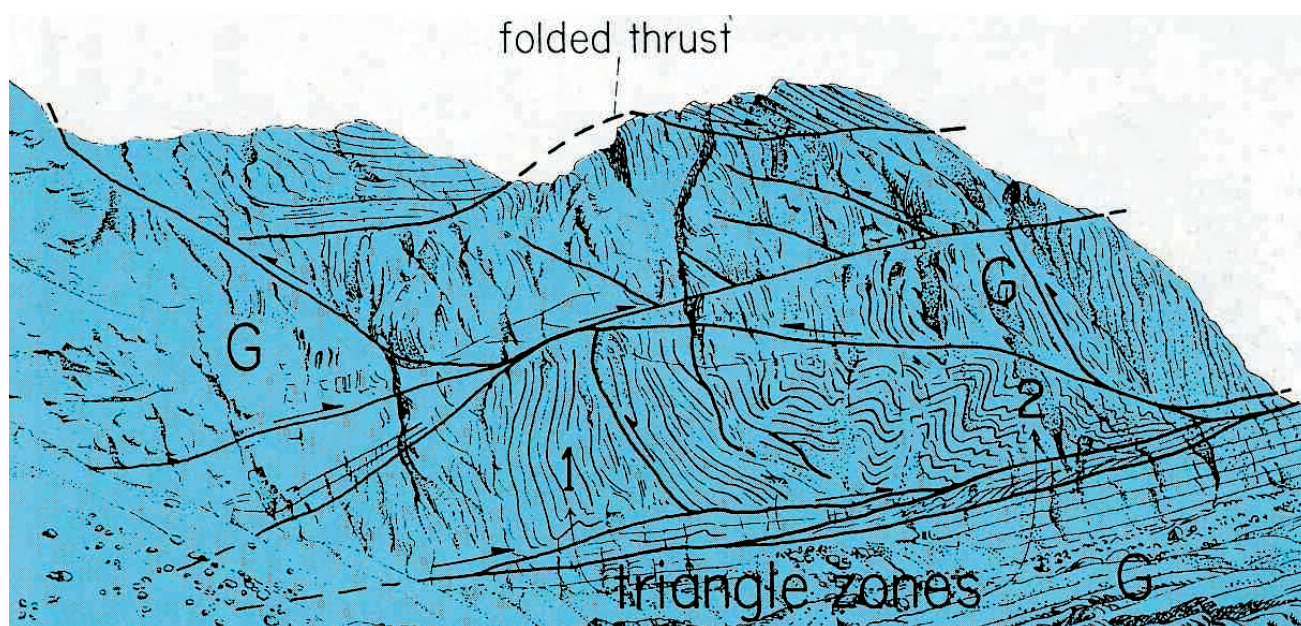
Fig. 86 - Examples of triangle zones in the Civetta Massif (Van dei Sass, central Dolomites). Numbers indicate the kinematic progression of the triangles. Front of the WSW-vergent Paleogene belt. G, Liassic Calcari Grigi.
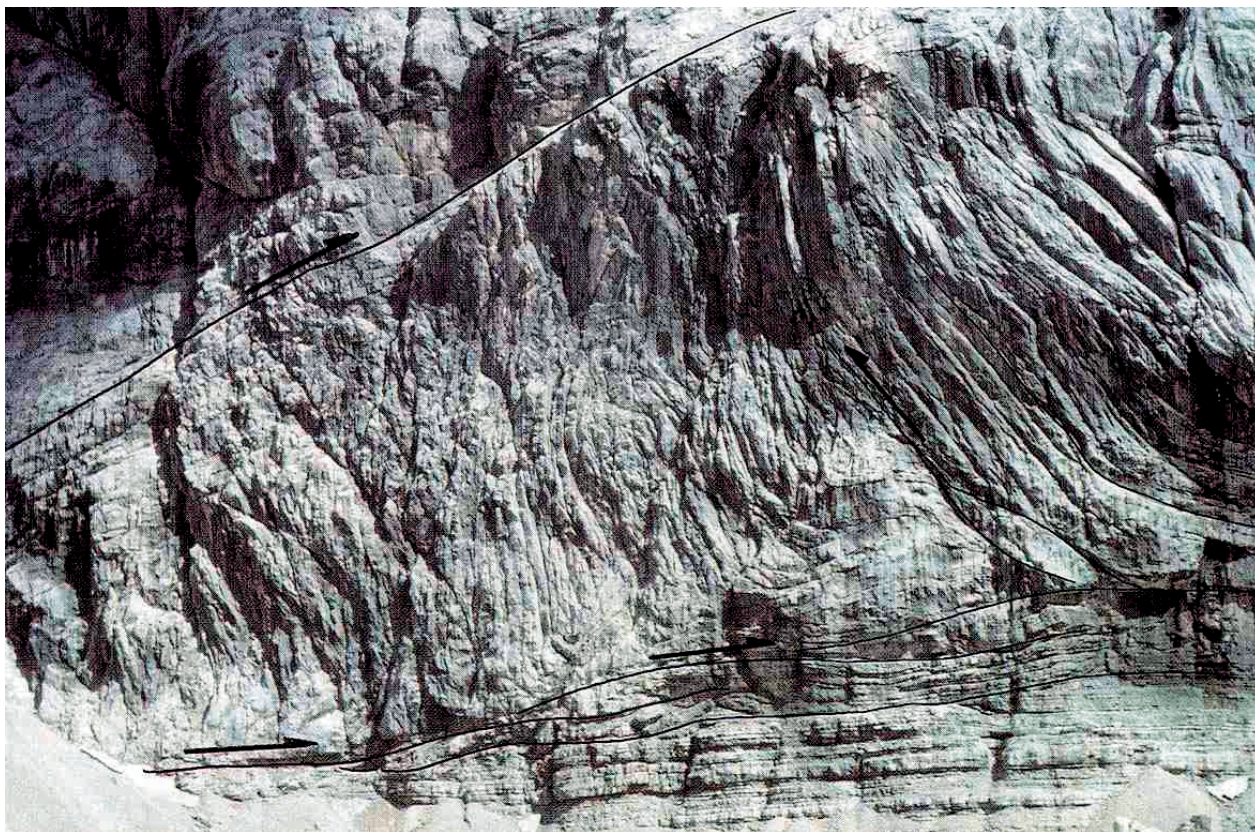
Fig. 87 - Detail of the central part of the previous picture. Triangle structure in Liassic Calcari Grigi, Van Dei Sass, Civetta Massif. The backthrust on the right side is folded and tilted.

Fig. 88 - Triangle structure developed in Carboniferous Rocks. Front Ranges of the Canadian Rockies. After SHAW *et alii* (2005) AAPG©, reprinted by permission of the AAPG whose permission is required for further use.